# REPORT DOCUMENTATION PAGE

Form Approved OMB No. 0704-0188

Public reporting burden for this collection of information is estimated to average 1 hour per response, including the time for reviewing instructions, searching existing data sources, gathering and maintaining the data needed, and completing and reviewing the collection of information. Send comments regarding this burden estimate or any other aspect of this collection of information, including suggestions for reducing the burden, to Department of Defense, Washington Headquarters Services, Directorate for Information Operations and Reports (0704-0188), 1215 Jefferson Davis Highway, Suite 1204, Arlington, VA 22202-4302. Respondents should be aware that notwithstanding any other provision of law, no person shall be subject to any penalty for failing to comply with a collection of information if it does not display a currently valid OMB control number.
**PLEASE DO NOT RETURN YOUR FORM TO THE ABOVE ADDRESS.**

| 1. REPORT DATE *(DD-MM-YYYY)* | 2. REPORT TYPE | 3. DATES COVERED *(From – To)* |
|---|---|---|
| 09-07-2007 | Final Report | 6 December 2005 - 29-November 2007 |

**4. TITLE AND SUBTITLE**

Compact Solid State Terahertz Detectors

**5a. CONTRACT NUMBER**
FA8655-06-1-3007

**5b. GRANT NUMBER**

**5c. PROGRAM ELEMENT NUMBER**

**6. AUTHOR(S)**

Professor Paul Harrison

**5d. PROJECT NUMBER**

**5d. TASK NUMBER**

**5e. WORK UNIT NUMBER**

**7. PERFORMING ORGANIZATION NAME(S) AND ADDRESS(ES)**

University of Leeds
Woodhouse Lane
Leeds LS2 9JT
United Kingdom

**8. PERFORMING ORGANIZATION REPORT NUMBER**

N/A

**9. SPONSORING/MONITORING AGENCY NAME(S) AND ADDRESS(ES)**

EOARD
Unit 4515 BOX 14
APO AE 09421

**10. SPONSOR/MONITOR'S ACRONYM(S)**

**11. SPONSOR/MONITOR'S REPORT NUMBER(S)**
Grant 06-3007

**12. DISTRIBUTION/AVAILABILITY STATEMENT**

Approved for public release; distribution is unlimited.

**13. SUPPLEMENTARY NOTES**

**14. ABSTRACT**

This report results from a contract tasking University of Leeds as follows: Within the frame of this project attention will be focussed on the low-frequency noise of the proposed devices. More specifically, the Johnson and shot noise, as well as 1/f noise spectra, will be measured at various temperatures from 4 K up to 300 K. The figure of merit commonly used to quantify the signal to noise ratio in infrared detectors is called the detectivity. This quantity, defined as the root-mean-square signal-to-noise ratio in a 1 Hz bandwidth per unit incident power per square root of the detector area, will be estimated under different bias voltages across the above temperature range.

Two design, fabrication and optimisation cycles will be completed in 12 months. Each cycle will begin with workers at Leeds designing the delta-doped FET layers and submitting the complete layer structures for growth in their new GaAs MBE facility. Parts of the as-grown wafers will be sent to Manchester for the optical characterisation while a researcher at Leeds will fabricate the device structures. Following this some of the devices will be dispatched to Vilnius for the electro-optic characterisation. This will involve measuring the Terahertz photocurrent at a range of temperatures and wavelengths. The results of the characterisation will be used to influence the second cycle of device designs.

The deliverables of the project will be low temperature electro-optic
characterisation of the photon detector at Terahertz wavelengths, a
mid-term progress report and a final report including a `roadmap' for the eventual development of single photon devices and prototype focal-plane-arrays of Terahertz detectors for operation with electro-thermal coolers at around 80 K.

Vilnius will supply an experimental Postdoctoral Researcher
for the full 12 months of the project. Leeds will supply 2 months of a Postdoctoral Research Assistants to design the devices, wafer growth and device fabrication costs. . Manchester will contribute to the optical characterisation of the device with Raman spectroscopy, photoluminescence (PL) and Fourier Transform InfraRed (FTIR)studies

**15. SUBJECT TERMS**

EOARD, terahertz detection, terahertz electronics, terahertz technology

| 16. SECURITY CLASSIFICATION OF: | | | 17. LIMITATION OF ABSTRACT | 18, NUMBER OF PAGES | 19a. NAME OF RESPONSIBLE PERSON |
|---|---|---|---|---|---|
| a. REPORT | b. ABSTRACT | c. THIS PAGE | | | A. GAVRIELIDES |
| UNCLAS | UNCLAS | UNCLAS | UL | 49 | 19b. TELEPHONE NUMBER *(Include area code)* +44 (0)20 7514 4953 |

# Compact Solid State Terahertz Detectors
# Final Report
# Contract: FA8655-06-1-3007

Paul Harrison[1], Gintaras Valušis[2] and Ed Linfield[1]

[1]*School of Electronic and Electrical Engineering, University of Leeds, LS2 9JT*
[2]*Semiconductor Physics Institute, A. Goštauto 11, 01108 Vilnius, Lithuania*

This effort was sponsored by the Air Force Office of Scientific Research, Air Force Material Command, USAF, under grant number FA8655-06-1-3007. The U.S. Government is authorized to reproduce and distribute reprints for Government purpose notwithstanding any copyright notation thereon

The views and conclusions contained herein are those of the authors and should not be interpreted as necessarily representing the official policies or endorsements, either expressed or implied, of the Air Force Office of Scientific Research or the U.S. Government.

I certify that there were no subject inventions to declare during the performance of this grant.

## Table of contents

# Introduction

As documented in the earlier reports, we have performed spectroscopic studies of the absorption of far-infrared or Terahertz radiation by impurities in semiconductor quantum wells. The absorbing transition occurs through the excitation of either an electron bound to a donor or a hole bound to an acceptor. Thus unlike typical semiconductor devices where the dopants are there merely to provide mobile electric charge, in these devices the dopants behave more like single atom quantum dots, hence the term `single atom quantum dot infrared photodetectors (SAQDIPs). Following the absorption of a photon the excited charge carrier can then be thermally ionised from the excited but still bound state of the impurity. The device concept developed in this programme was to have such a system of absorbing impurity states in the presence of a lateral (parallel to the plane of the quantum wells) electric field which then sweeps away the photo-carriers to form a photocurrent. The role of the quantum well potential is to enable some adjustment in the impurity binding energy and hence the wavelength of the peak in responsivity.

p-type dopants, in particular Beryllium (Be) which has a binding energy in bulk GaAs of 28 meV was found to be the most suitable for detection in the technologically interesting terahertz frequencies. The 28 meV corresponds to the direct ionisation energy of a hole from the impurity ground state to the continuum level associated with the ground state subband of the quantum well, in fact absorption will occur when the photon energy is sufficiently large to excite the hole from the 1s impurity level to the 2p. The latter occurs at ¾ of the value of the binding energy i.e. 21 meV which is equivalent to around 60 microns wavelength. Photocurrent may also originate at these frequencies if the hole is thermally dissociated before it relaxes back to the 1s ground state.

## Summary of Terahertz photocurrent spectroscopy of beryllium δ-doped GaAs/AlAs quantum well devices

To test the operation within THz range, we have measured the THz radiation-induced photocurrent in an in-plane geometry of the samples at liquid helium temperatures. The results are depicted in Fig. 1. The origin of the signal we associate mainly with photothermal ionization of Be acceptors as the increasing edge in the photoresponse corresponds to the acceptor binding energy. The results of the measurements of two earlier samples (1392 and 1794) grown before this project are included for comparison. Sample 1392 had two orders of magnitude higher doping than sample 1794 and hence produced a significantly higher signal because of the increased THz absorption. The signal observed below 4 THz can be related to excited acceptor states $2P_{3/2}$ and $2P_{5/2}$ having transition energies several meV lower than the binding energy [1].

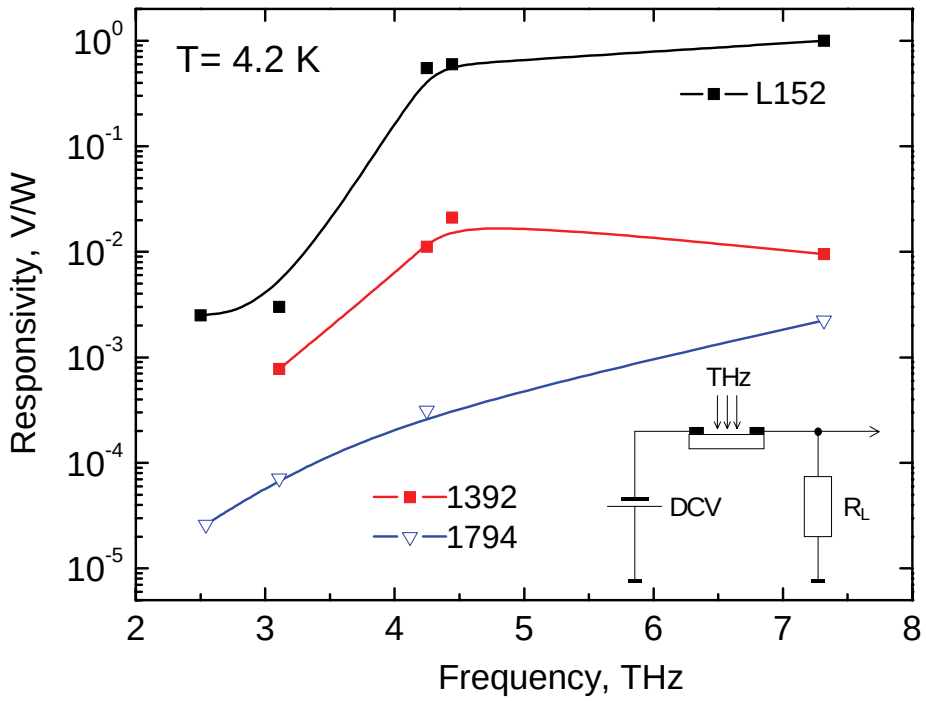


**Fig. 1** Photovoltage responsivity of the δ-doped GaAs/AlAs MQW-based devices recorded across the THz range at helium temperatures.

Sample L152 produced the best performance of the devices fabricated for this project. It can be seen from Fig. 1 that in this project by switching the sample supply to our new in-house MBE facility in Leeds which is aimed at producing the highest quality semiconductor layers and by improving the device fabrication we have been able to increase the responsivity, i.e. in this case the photovoltage per unit incident power, by an amount which increases from a factor of 50 at 4 THz (75 microns wavelength) to 100 at 7 THz (43 microns).

## Comments on noise

We think that the noise in our Be doped GaAs quantum well structures is of the shot noise origin as in conventional GaAs QWIPs designed for mid-infrared detection (see for example J. Appl. Phys. **70**, 5101 (1991)). If this is the case, then noise current can be calculated according to the equation (see the same reference):

$$i_n = \sqrt{4eI_D g\Delta f}$$

where $I_D$ is the dark current, $g$ is the optical gain and $\Delta f$ is the measurement bandwidth. In QWIPs $g$ is usually less than unity and within the range 0.3-0.6, therefore the measured current noise is slightly less than full shot noise given by $\sqrt{4eI_D\Delta f}$ (again see J. Appl. Phys. **67**, 7608 (1990)).

The actual value of $g$ is not yet known in our structures but for the purpose of these simple noise calculations, we can take it as approximately unity. We found that at a temperature of 4 K and a bias voltage of 10 V the dark current in our Be doped GaAs samples is around 40 pA, see Fig. 2. Note the sample is cut from the 300 K background radiation with a copper shield kept at 4 K. In this case, the dark current shot noise would be equal to 5 fA/√Hz.

Normally, in a detection application a hole must be opened in the cold shield to allow the THz radiation in. At the same time background radiation also reaches the sample increasing the dark current and also the current noise. The increase in the dark current depends on the hole diameter, more specifically, on the field of view angle. Therefore, the dark current noise must be re-evaluated for each specific application geometry.

Following on from this the noise equivalent power in the detectors at liquid helium temperatures is in the range of 5 nW/Hz$^{1/2}$.

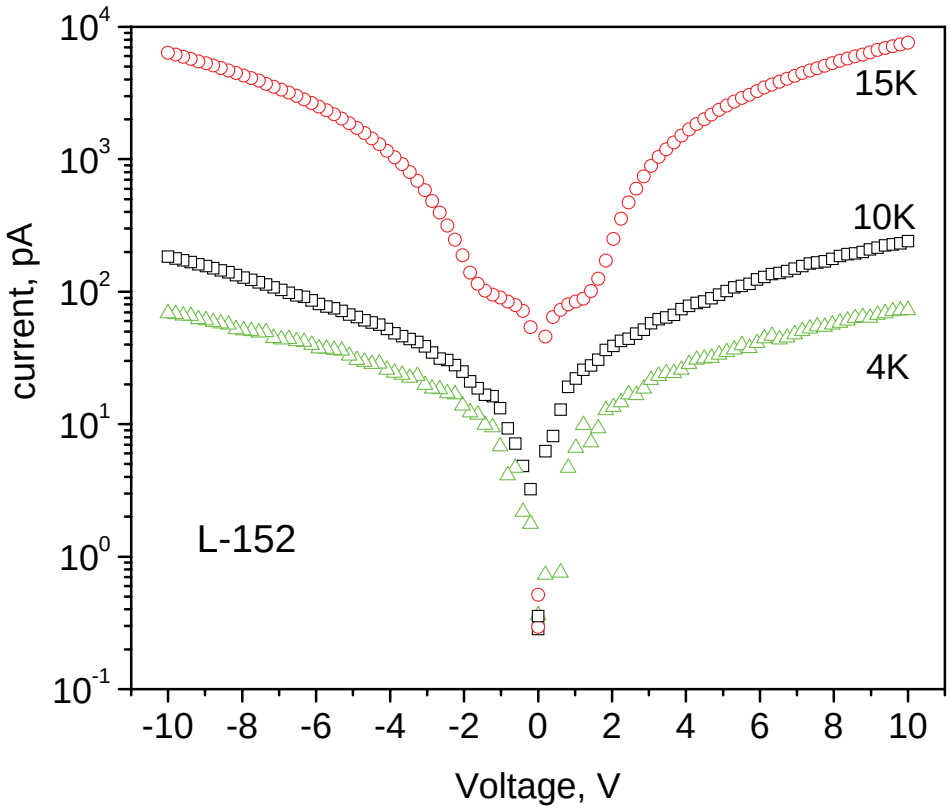


**Fig. 2.** The dark current-voltage characteristics of sample L152 at different lattice temperatures

## Summary of device performance

Estimates of the photocurrent responsivity have shown peak values of around 0.1 mA/W at 41 microns wavelength in the sample L152. This indicates that there is still some way to go for these SAQDIP devices to catch up the performance of state-of-the-art far-infrared solid state detectors (e.g. the HEIWIP device of Perera et al., Appl. Phys Lett. 78, 2241 (2001) gave a responsivity of 0.7 A/W at 40 microns and 0.007 A/W at 70 microns). However, the progress made in this project is encouraging and there are still avenues to try to improve things further. For example, the doping of sample L152 was deduced to be around $5x10^{11}$ $cm^{-2}$. We believe, through calculations and measurements, that the Be acceptors will retain their quantum dot-like properties up to the metal-insulator transition which occurs around $5x10^{12}cm^{12}$, so we have the potential for up to an order of magnitude increase in the doping level which we expect to lead to similar improvements in the responsivity. Therefore we can improve the absorption cross-section of the devices by increasing the doping density in each well, as long as we stay below the Mott limit. However, L152 was grown with 60 quantum well periods, so the absorption cross-section can be increased further by increasing the total sheet doping density, i.e. by increasing the number of quantum wells. We believe that this number of active layers can easily be doubled or tripled. When both of these factors are combined together they indicated that a further factor of 20-30 improvement over and above that produced in this work, is feasible. This would then improve upon the low temperature performance of HEIWIPs.

## Roadmap for future development

Single-pixel optimization:

- Further explorations of optimum doping density: 5 MBE samples
- Optimisation of the number of active (absorbing) layers: 5 MBE samples
- Development of resonant cavity for improved coupling of incident radiation and absorption centres: 3 MBE samples
- Optimisation of interdigitated contacts (`gate' length and spacing) for greater photocurrent collection (improved photoconductive gain)

This would need to be a two year long programme at the level of a dedicated postdoctoral research assistant to design, fabricate and carry out the basic characterization at Leeds. A further, probably 50%, part-time researcher would be required in Vilnius to complete the terahertz spectroscopy measurements.

# Compact Solid State Terahertz Detectors: First interim report Contract: FA8655-06-1-3007

P. Harrison,
School of Electronic and Electrical Engineering,
University of Leeds, Leeds LS2 9JT, United Kingdom

February 6, 2006

The aims of the project are to design, fabricate and characterise *p*-type semiconductor heterostructures as terahertz detectors. The detectors are designed to absorb photons through intra-impurity transitions which liberate holes (positive charge carriers) which are then swept to electrical contacts by a d.c. bias. The planned time-line for the project overall is given in Table 1.

Designing the semiconductor layer structures to be grown was the clearly the first priority and with this aim a meeting with Gintaras Valušis and co-workers in Vilnius was held to review all our earlier work and agree the likely optimium layer structure for the electronic and optical properties of the devices. A subsequent discussion with Ed Linfield, the leader of the growth facility at Leeds, further informed the designs of the growth envelope and the layer structure for the first prototype cycle, illustrated schematically in Fig. 1, was settled upon.

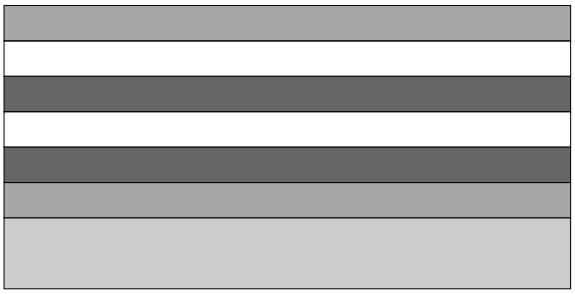


Figure 1: Schematic diagram of the layer structure of the semiconductor heterostructures. The GaAs quantum wells are to be modulated doped to yield carrier densities per period of $5\times10^{10}$, $5\times10^{12}$ and $10^{13}$ cm$^{-2}$.

The meeting in Vilnius also covered the requirements for the electro-optic characterisation, preparations for which are now under way. In the meantime the 3 semiconductor samples, differing by doping density, have been submitted for growth by molecular beam epitaxy.

# Project Timetable

Table 1:

| | Month 1-2 | Month 3-4 | Month 5-6 | Month 7-8 | Month 9-10 | Month 11-12 |
|---|---|---|---|---|---|---|
| Literature search | * | * | * | * | * | * |
| Device design | * | | | | | |
| Electro-optic system preparation | * | * | | | | |
| Device fabrication | | | * | | | |
| Optical characterisation | | | * | | | |
| Electro-optic characterisation | | | | * | | |
| PROJECT MEETING IN VILNIUS | | | | * | | |
| Device design | | | | * | | |
| Device fabrication | | | | | * | |
| Optical characterisation | | | | | * | |
| Electro-optic characterisation | | | | | | * |
| PROJECT MEETING IN LEEDS | | | | | | * |
| FINAL REPORT | | | | | | * |

# Compact solid state terahertz detectors: design of active structures and their optical properties

Second interim report

Contract: FA8655-06-1-3007

# Introduction

The Terahertz (THz) ($1-10\times10^{12}$ Hz or equivalently 300−30 $\mu$m wavelengths) region of the electromagnetic spectrum lies between microwaves (exploited in mobile phones, satellite communications, television) and the infrared (used in heat sensing, short-range data communications) and is still largely unexplored and unexploited. Despite the large potential applications in such areas as bio-medical imaging (diagnosis of melanomas, drug levels in blood, DNA profiling, detection of bacterium and viruses), detection of chemical signatures (airport security, food hygiene, textiles) and satellite communications, to name a few, there is an obstacle in the way of the development of this frequency range – namely that in this region the well-known principles of both photonics and electronics are no longer working. That is why a development of compact THz devices requires confluence of various technologies and establishment of novel principles.

Quite recently, the *THz Atelier* group from Vilnius, in co-operation with Frankfurt/M (Germany) and Montpellier (France) groups has explored two principles devoted to broad band detection using semiconductor nanostructures containing two-dimensional electron gases (2DEG). The first way is to excite plasma waves in a 2DEG layer embedded in a field-effect transistor (FET) with a submicron length gate. For instance, CMOS transistors with a gate length of 30 nm can detect at 2.52 THz [1]. The other approach is based around non-uniform carrier heating in 2DEG layers in GaAs/AlGaAs modulation doped structures in specifically engineered devices. These so-called bow-tie diodes (due to similarity of their shape to a bow-tie antenna) reveal an operating bandwidth from 10 GHz−2.52 THz [2]. The inherent feature of the diodes is a *plateau* in the voltage sensitivity across the 10 GHz−0.8 THz range with a value around 0.3 W/V. For direct applications, however, one needs to investigate a photon detection scheme which is free from the selection rules limitation inherent for THz QWIPs (quantum well infrared photodetectors) [3].

This problem is the main inspiration of the given work. The object of the investigation is *p* (Be)- and *n* (Si)- δ-doped GaAs/AlAs quantum wells with different

well widths and various doping levels. The study presents comprehensive research, both theoretical and experimental, by optical (modulation spectroscopy and photoluminescence), electrical and terahertz photocurrent techniques across the 4−300 K temperature range.

## Design of Be and Si δ-doped GaAs/AlAs quantum wells

Delta-doped GaAs/AlAs multiple quantum wells (MQWs) were grown by molecular beam epitaxy (MBE) on semi-insulating (100) GaAs substrates with a 300 nm GaAs buffer. Each of the MQW structures investigated (samples designated as 1807, 1392, L29, L30 and L45) contained 20 nm wide GaAs quantum wells (QWs) separated by 5 nm wide AlAs barriers. The QWs were δ-doped at the well centre with Be acceptor or Si donor atoms. The first 100-period GaAs/AlAs MQW structure (sample 1807) was weakly doped with acceptor density of $5\times10^{10}$ cm$^{-2}$. The second a 40-period MQW structure (sample 1392) was highly doped with Be acceptors of density $2.5\times10^{12}$ cm$^{-2}$. The 40-period MQW structures L29, L30 and L45 were relatively weakly doped with Si in the range from $4\times10^{9}$ to $1.4\times10^{11}$ cm$^{-2}$ and the structures were capped with a 100 nm GaAs layer. The doping level and the main characteristics of each sample are summarized in Table I.

The schematic band diagram of the δ-doped GaAs/AlAs MQW structures has been calculated using Poisson's and Schrödinger equations, the results of which are

**Table I.** Characteristics of the samples: the number of periods, the quantum well width ($L_w$), the δ-doping Be (Si) concentration $N_A$ ($N_D$) and the growth temperature of the epitaxial layer ($T$).

| Samples | Periods | $L_w$ (nm) | $N_A$ (cm$^{-2}$) | $T$ (ºC) |
|---|---|---|---|---|
| 1794 | 200 | 10 | $5\times10^{10}$ | 550 |
| 1303 | 50 | 15 | $2.5\times10^{12}$ | 540 |
| 1392 | 40 | 20 | $2.5\times10^{12}$ | 540 |
| 1807 | 100 | 20 | $5\times10^{10}$ | 550 |
| Samples | Periods | $L_w$ (nm) | $N_D$ (cm$^{-2}$) | $T$ (ºC) |
| L29 | 40 | 20 | $4\times10^{9}$ | 670 |
| L30 | 40 | 20 | $1.4\times10^{11}$ | 670 |
| L45* | 40 | 20 | $5\times10^{16}$ (cm$^{-3}$) | 705 |

*For sample L45, the Si doping was in the centre 2 nm of 20 nm GaAs quantum well.

shown in Fig. 1. We have assumed that the surface Fermi level for the *p*-type GaAs is pinned at 0.5 eV above the valence band. Consequently, this results in the formation of a surface depletion layer and a surface electric field. Another depletion layer is also formed at the interface between the MQW layer and the substrate due to Fermi level pinning near the middle of the bandgap of the semi-insulating GaAs.

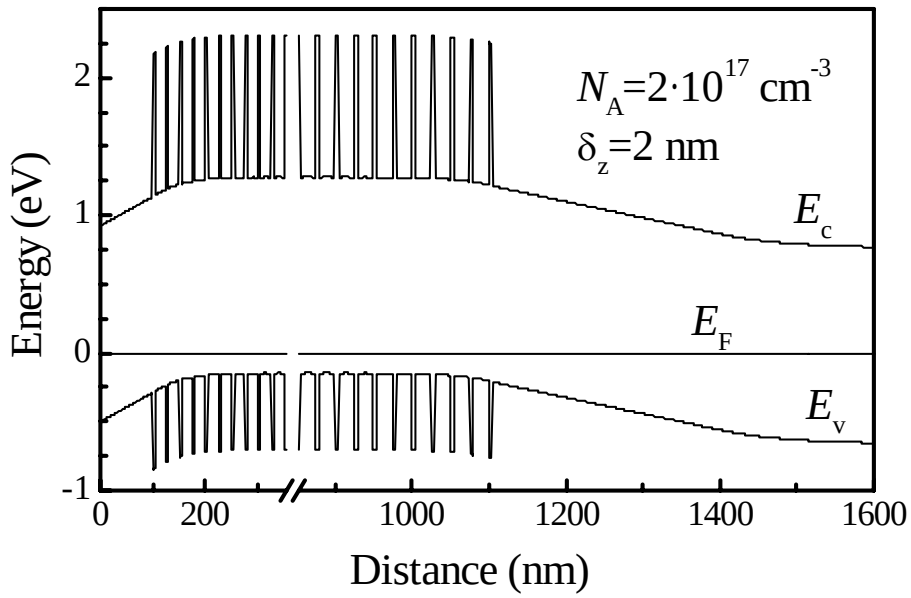


Fig. 1. The calculated band diagram of a beryllium (Be) δ-doped MQW structure. $E_c$ and $E_v$ are the conduction and valence band edges. $\delta_z$ is the width of the Be-doped layer.

## Optical properties of δ-doped GaAs/AlAs quantum wells: A study by modulation spectroscopy

The strong interest in *δ*-doped semiconductor nanostructures is motivated by the possibility of using them as active media in future THz electronic and photonic devices. The non-destructive characterization of complex multilayer structures is a crucial step in the fabrication of semiconductor devices. Optical modulation spectroscopies such as differential surface photovoltage (DSPV), photoreflectance (PR) and contactless electroreflectance (CER) are powerful tools to evaluate the performance of semiconductor heterostructures [4-8].

The first project period was focused on DSPV spectroscopy of nanostructures. The main objectives were: (1) to develop the DSPV technique as well as spectral line shape analysis methods for investigation of interband optical transitions and electronic states in nanostructures; (2) to study SPV and DSPV spectra of Be and Si $\delta$-doped GaAs/AlAs multiple quantum wells (MQWs); (3) to calculate the QW energy levels in order to disclose the nature of optical transitions and spectral line broadening mechanisms as well as the structural quality of $\delta$-doped GaAs/AlAs MQWs.

## Study of δ-doped GaAs/AlAs MQWs by DSPV spectroscopy

The energy levels of Be acceptors or Si donors embedded in GaAs/AlAs quantum wells (QWs) can be tuned across the terahertz (THz) range by changing the width of the GaAs quantum well [9, 10]. This is relevant for detectors and emitters in THz electronics. Nevertheless, well-width fluctuations (interface roughness) of MQWs will result in the inhomogeneous broadening of electronic states [11]. For technological development of electronic devices such inhomogeneities are of critical importance and must be kept as small as possible. Thus, knowledge about the structural disorder of $\delta$-doped GaAs/AlAs MQWs is particularly important for improving the quality of heterostructures. A great deal of useful information concerning structural inhomogeneities of low-dimensional semiconductor structures can be obtained from the study of excitonic linewidths which are very sensitive to disorder [6, 11] and may be a key factor in improving the performance of THz devices.

In this work, room- and low-temperature (90 K) differential surface photovoltage (DSPV) was used to study the excitonic transitions in Be and Si $\delta$-doped GaAs/AlAs MQW structures. Analysis of the lineshape of the DSPV spectra allowed us to extract information on the excitonic parameters for a large number of QW subbands. Special attention was paid to examination of exciton line broadening which is directly related to the structural quality of MQW systems.

**Experimental setup**

SPV measurements were performed in a chopped light geometry (Fig. 2) by using a capacitor-like system with a transparent conducting top electrode under normalized incident light intensity conditions [12]. The samples were mounted on copper plate, which acts as the back electrode. The top conducting electrode was an indium-tin-oxide (ITO) coated glass plate. Light from a 100 W tungsten halogen lamp was passed

through a grating monochromator SPM-2 and focused onto the sample. The illumination intensity was selected at sufficiently low levels in order not to affect the line shape of the spectra. In DSPV spectra measurements, we have used a wavelength-modulation technique [13]. The wavelength $\lambda$ of the incident probe light was modulated by vibrating a fused-silica plate at 87 Hz located near the exit slit of the monochromator. Typically $\Delta\lambda/\lambda$ was on the order of $10^{-3}$. The alternating-current (ac) signal generated by a chopped light beam in SPV measurements or by a wavelength-modulated light beam in the DSPV experiments were recorded by a conventional lock-in detection system. The measurements were performed at 90 and 300 K.

Figure 3 shows the DSPV spectrum measured with the wavelength-modulation technique and the numerically computed first derivative of the SPV spectrum with respect to the photon energy *E*, d(SPV)/d*E*. As can be seen, there is excellent agreement between the measured DSPV spectrum and the numerical derivative d(SPV)/dE. This provides evidence that the results of wavelength-modulated DSPV in

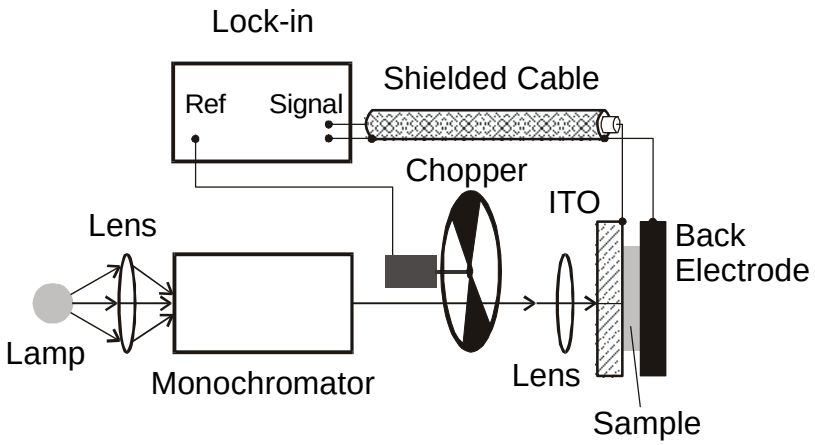


Fig. 2. Schematic diagram of the experimental setup for SPV and DSPV measurements

$\delta$-doped GaAs/AlAs MQWs are dominated mainly by photon energy modulation and the spurious signal from light intensity modulation is negligible.

**Line-shape analysis of DSPV spectra**

The SPV spectra of $\delta$-doped GaAs/AlAs MQWs were interpreted taking into account the fact that two oppositely directed internal electric fields exist in the structures, one in the cap layer and one in the buffer layer (see Fig. 1). In this case, the total SPV signal should be considered as a superposition of the two signal components with opposite sign [8]. We found that the SPV signal component coming from the interface region of the GaAs buffer layer is dominant. Since the GaAs cap layer is relatively thin, the SPV signal arises mostly due to light absorption in the GaAs buffer layer of the MQW sample. Light absorption does also takes place in the QWs. Consequently, it is very likely that the features observed in the SPV spectra at the energies above the GaAs band gap arise mainly due to the attenuation of incident light passing through the MQW layer at the exciton resonances [14]. Therefore, the SPV spectrum above the GaAs band gap energy resembles a transmission spectrum of the MQW layer.

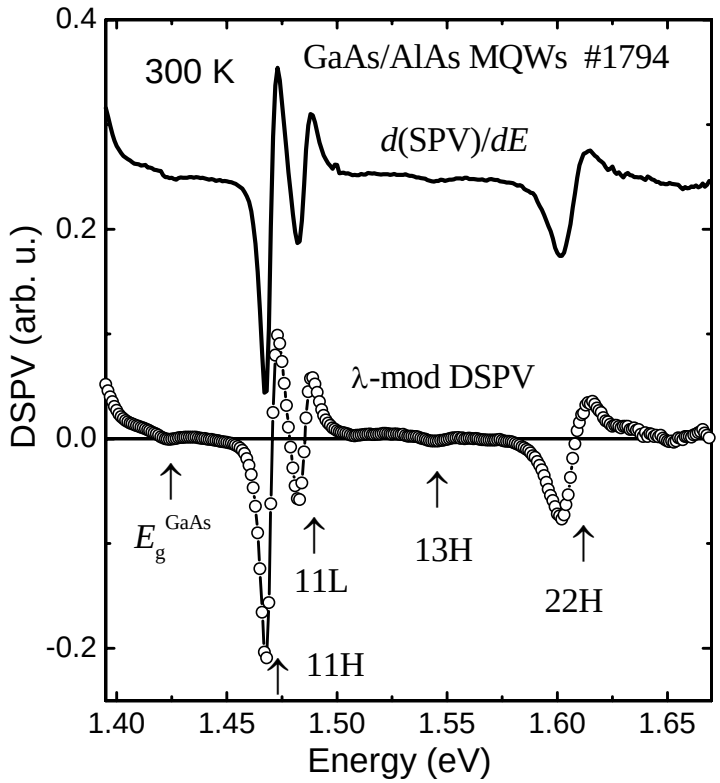


FIG. 3. A comparison of experimentally measured λ-modulated DSPV (bottom, open circles) and the numerically computed first derivative of the SPV spectrum (top, solid curve) for the GaAs/AlAs MQW sample 1794 at room temperature.

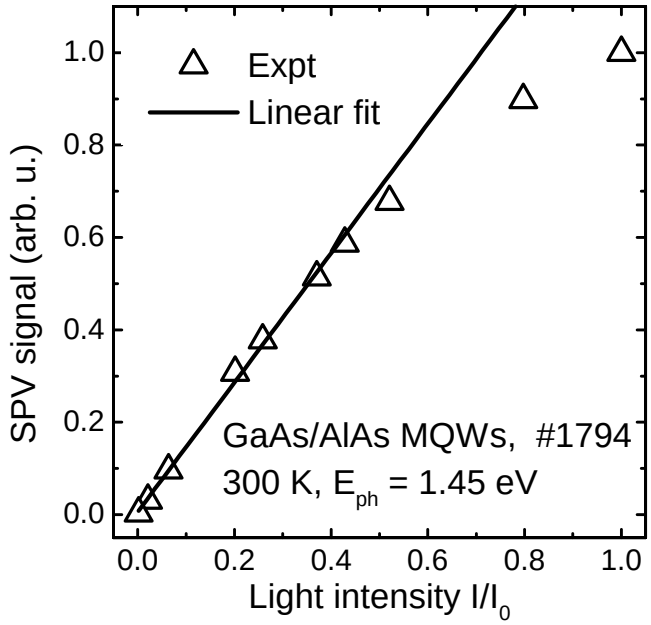


FIG. 4. The dependence of the SPV signal amplitude on the relative light intensity at the photon energy 1.45 eV for the GaAs/AlAs MQW sample 1794.

The excitonic features in the DSPV spectra were analysed on the basis of the model assuming that normal-incident SPV features for MQWs are related to photoabsorption. We suppose that the spectral responsivity of the buried interface region above the GaAs band-gap energy is slowly varying with wavelength, compared to the sharp spectral lines of the optical transitions in the MQW. In this case, neglecting the spectral dependence of the reflectivity, the measured quantity d$V$/d$E$ of DSPV should be related to the first derivative of the absorption coefficient $\alpha$ of the MQW layer versus photon energy $E$ [15]

$$\frac{1}{V}\frac{\mathrm{d}V}{\mathrm{d}E} \sim \frac{1}{d_w}\frac{1}{I}\frac{\mathrm{d}I}{\mathrm{d}E} = -\frac{\mathrm{d}\alpha}{\mathrm{d}E}, \qquad (1)$$

where $V$ is SPV signal, $d_w$ is thickness of MQW absorbing layer, and $I$ is the light intensity absorbed in the GaAs buffer layer.

We found experimentally that the SPV amplitude above the GaAs band gap energy increases linearly with the excitation intensity under weak illumination and tends to saturate at strong illumination (Fig. 4). Therefore, for the regime of weak excitation (d$V$~$I$), the wavelength dependence of the SPV above the GaAs band gap can be related to the spectral dependence of the absorption coefficient of the MQW layer. In this case the normalized DSPV, (d$V$/d$E$)/$V$, spectra are qualitatively equivalent to the first derivative of the absorption spectra [15].

The energies and broadening parameters of optical transitions responsible for the observed DSPV features (Fig. 3) were determined from the fit of the DSPV spectra to the derivative functional form proposed by Aspnes [16]:

$$(dV/dE)/V = \mathrm{Re}\left[Ce^{i\theta}\left(E - E_g + i\Gamma\right)^{-m}\right], \qquad (2)$$

where $C$, $\theta$, $E_g$ and $\Gamma$ are the amplitude, phase, energy and broadening parameter of the spectral feature, respectively. The value of parameter $m$=2 was used in the calculations. It should be noted that in this case the expression (2) represents quite well the first derivative of an excitonic dielectric function with a Lorentzian absorption profile [4, 5], which is appropriate for excitonic transitions in QW structures.

## III. RESULTS AND DISCUSSION

### DSPV spectra

We first consider the results from the Be $\delta$-doped GaAs/AlAs MQWs. Figure 5 shows the typical DSPV spectra for the GaAs/AlAs MQW structures (samples 1807 and 1392) at 90 and 300 K. At energies higher than $E_g^{GaAs}$ (1.424 eV at 300 K and 1.507 eV at 90 K), the spectra are dominated by the optical features *mn*H(L) that could be associated with excitonic transitions in the MQW region of the samples. The notation *mn*H(L) signifies the transitions between the *m*-th electron and *n*-th heavy hole (H) or light hole (L) subbands. As mentioned above, by considering excitonic features we assumed that the spectra of the normalized DSPV/SPV signal, i.e. the ratio - $(dV_{SPV}/dE)/V_{SPV}$, are qualitatively equivalent to the first derivative of the absorption spectra. The energies and broadening parameters of the optical transitions responsible for the observed DSPV features were determined by best fits of the DSPV spectra to the first derivative of a Lorentzian-type function (2). As can be seen from Fig. 5, the experimental DSPV data (open circles) are reasonably well described by this line shape model (full lines) both at low and high temperature. The optical transition energies (arrows in Fig. 5) were found to change according to QW thickness as expected from the quantum confinement effect and also predicted by energy level calculations [6]. With decreasing temperature, the DSPV features shifted toward higher energies due to the increase in the band gap of the GaAs well layers. At 90 K,

the light- and heavy-hole transitions are well resolved owing to the smaller broadening of the energy states.

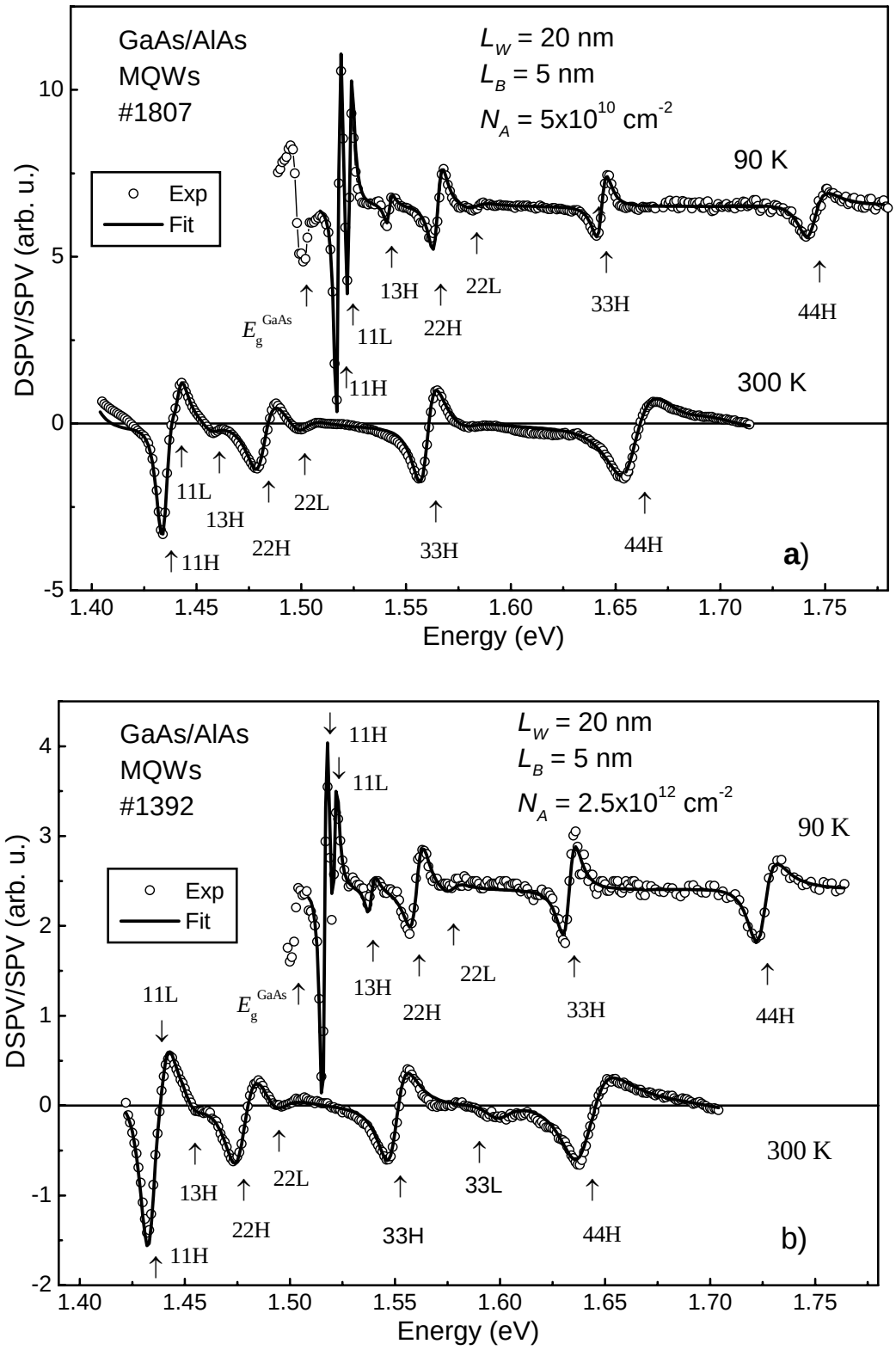


Fig. 5. DSPV spectra of Be δ-doped GaAs/AlAs MQWs at 90 and 300 K for weakly (a) and highly (b) doped samples. The arrows show the excitonic transitions energies obtained from the fit of experimental data (open circles) to the first derivative of a Lorentzian-type function (solid curves).

Let us now consider the results from Si δ-doped GaAs/AlAs MQWs. Figure 6 shows the SPV spectra of Si doped samples L29, L30 and L45 measured at room temperature under the same conditions. At low photon energies, these spectra exhibit a sharp increase in the photovoltage, which can be related to the onset of absorption in bulk GaAs layers. The shoulder around 1.38 eV in the spectra seems to be due to the impurities, while the knee at 1.42 eV is related to the GaAs band edge. At higher energies, pronounced discrete dips that could be associated with excitonic transitions in the MQWs are clearly visible. In order to study the QW-related optical transitions with higher resolution, we have measured the DSPV spectra. The DSPV data for three Si doped GaAs/AlAs MQW samples are shown by open circles in Fig. 7. In order to determine the interband transition energies and broadening parameters, a fitting procedure as described above, was performed. The fitting curves are shown with solid lines and the arrows correspond to transition energies determined from the fitting. It should be noted that no important differences between the DSPV spectra of different samples are observed. However, for the samples L30 and L45 the DSPV spectra are much broadened.

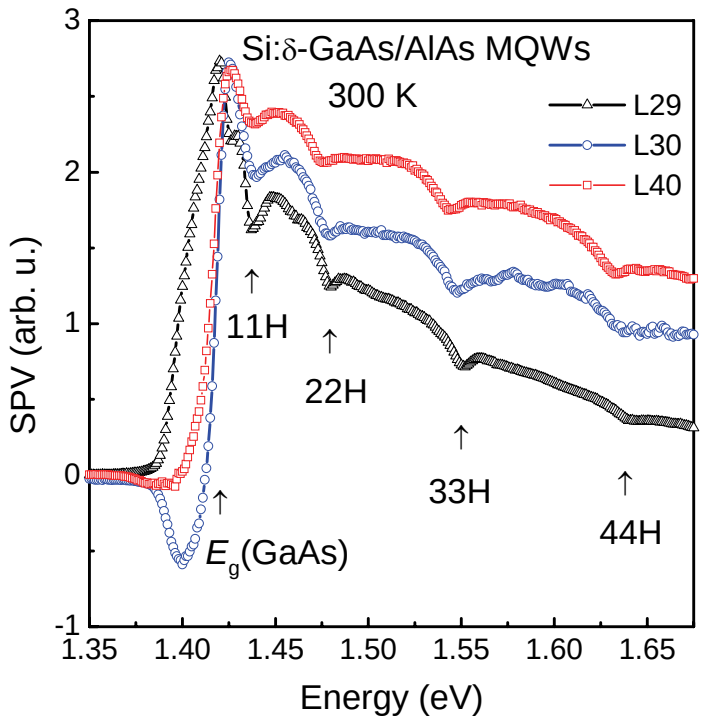


Fig. 6. Room temperature SPV spectra of Si doped GaAs/AlAs MQW samples L29, L30 and L45. Arrows indicate the energies of interband optical transitions in MQWs. All the spectra are normalized at the photon energy 1.42 eV.

**Subband structure and optical transitions**

To identify the spectroscopic data, we have carried out calculations of energy levels and interband transition energies for GaAs/AlAs QWs both for parabolic and non-parabolic energy bands in the envelope function approximation [17]. For the parabolic energy spectrum, the Schrödinger equation for carriers in a rectangular QW was solved numerically by the transfer matrix method [18] and also by using simple well-known dispersion relations for rectangular potential profiles [17]. Both calculating procedures yield, within 1-2 meV, almost the same values of the energy levels. Non-parabolicity effects were taken into account by using energy-dependent effective electron and light-hole masses [17]. At the conduction band edge, the

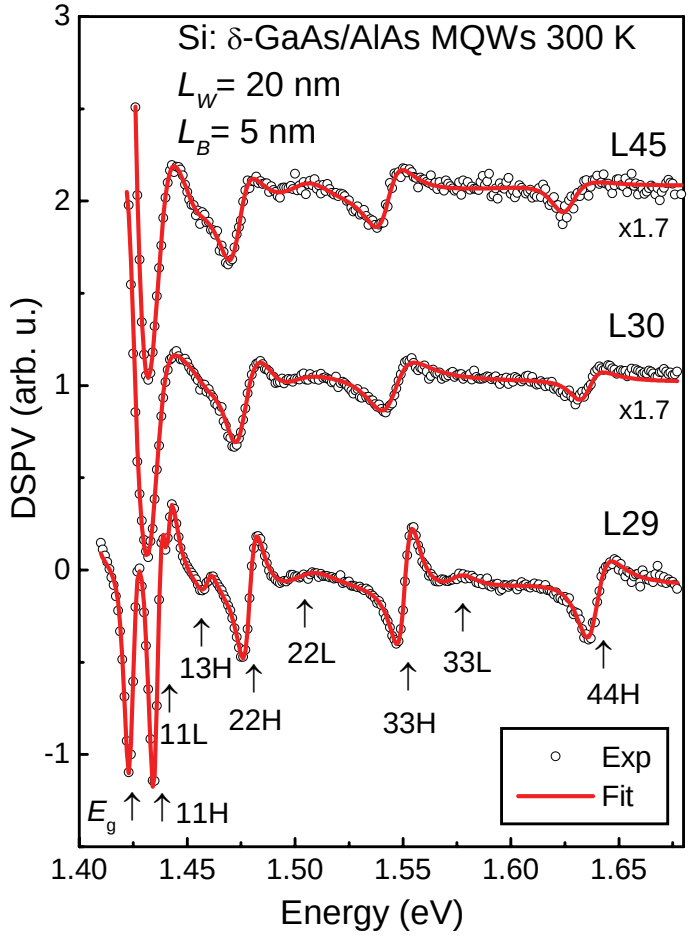


Fig. 7. Room temperature DSPV spectra of Si doped GaAs/AlAs MQW samples L29, L30 and L45. The transition energies indicated by arrows were obtained from the fit (solid line) of the first derivative of a Lorentzian-type function (2) to the experimental data (open circles).

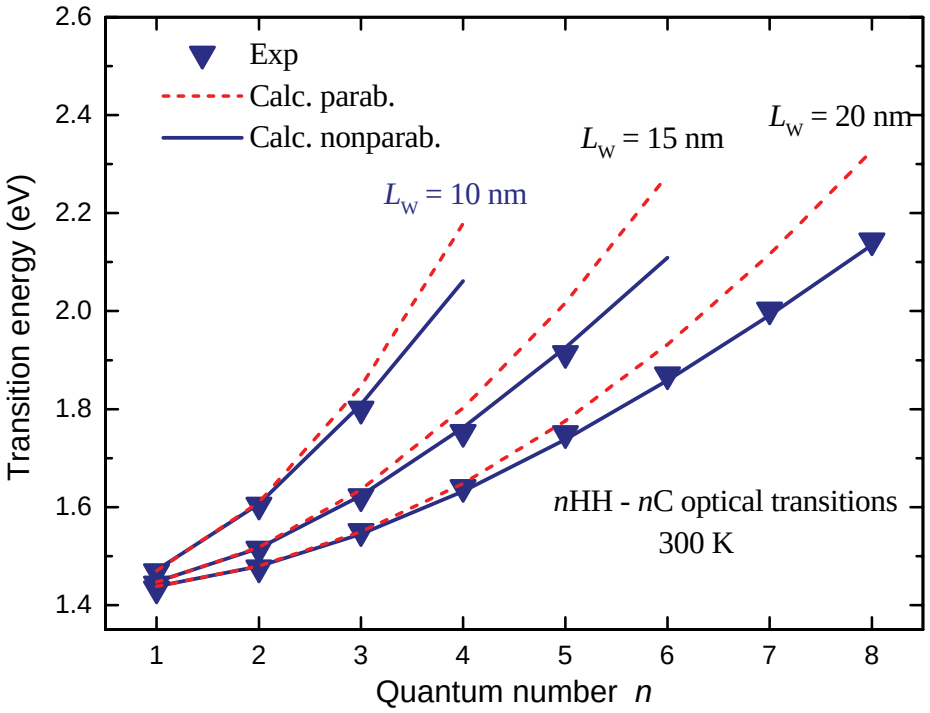


Fig. 8. Heavy-hole related excitonic transition energies as function of quantum number for Be $\delta$-doped GaAs/AlAs MQWs. The calculations were performed for parabolic (dashed curves) and non-parabolic (solid curves) energy band approximations.

effective masses of electrons, $m_e = 0.0635m_0$ in GaAs and $m_e = 0.15m_0$ in AlAs [16] were employed. At the valence band edge, the effective masses of heavy- and light holes along the $z$ direction were evaluated from Luttinger parameters $\gamma_1$= 6.98, $\gamma_2$=2.06 for GaAs and $\gamma_1$=3.76, $\gamma_2$=0.82 for AlAs [19]. The forbidden energy gap values $E_g^{\Gamma}$ = 1.424 and 3.018 eV [20] for GaAs and AlAs respectively, were used. The conduction band offset was taken to be 0.65. To check the assumption as to the rectangular potential profile of the QWs under consideration, calculations of the energy levels by solving coupled Poisson-Schrödinger equations have also been performed. It was found that the change in the ground state optical transition energy due to distortion of the rectangular QW potential profile by δ-doping is negligible and remains $\leq$ 3 meV when the concentration of acceptors is $2.5\times10^{12}$ cm$^{-2}$ and the width of the QW is 20 nm. For narrower QWs and higher order optical transitions the deviations were found to be even smaller.

The results of the calculations and the experimental data are presented in Fig. 8 and 9, where the dependencies of the transition energies on the quantum number are plotted for Be and Si doped GaAs/AlAs MQWs, respectively. The symbols represent the exciton energies determined from the fitting procedure, while the lines correspond

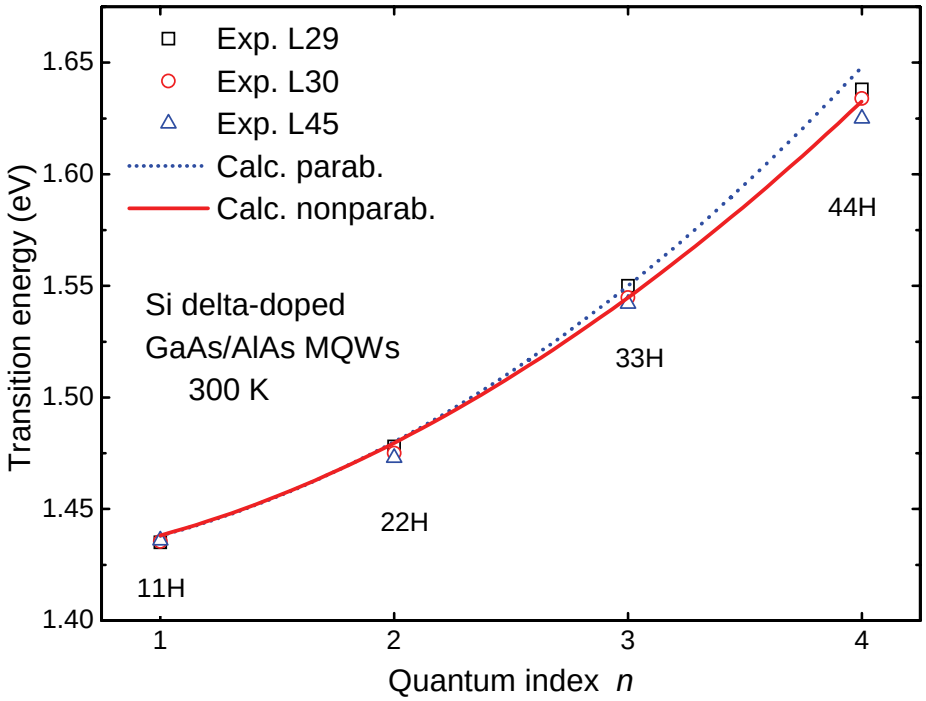


Fig. 9. The experimental (symbols) and calculated (lines) dependencies of heavy-hole related interband transition energies on quantum index $n$ for Si δ-doped GaAs/AlAs MQWs. The calculations were performed for parabolic (dashed curve) and non-parabolic (solid curve) energy bands approximation.

to theoretical results, obtained for the parabolic (dashed lines) and non-parabolic (solid lines) energy band approximations. It should be noted, that the experimental transition energies slightly differ at high quantum number $n$ for different Si doped GaAs/AlAs MQW samples (Fig. 9). This observation indicated that average well width $L_W$ could differ slightly from the nominal in this set of samples due to a possible technological inaccuracy.

As can be seen from Figs. 8 and 9 the parabolic band model predicts correctly the lowest transitions but overestimates the energies of the higher transitions. However, the experimental data are in quite good agreement with calculations performed by taking into consideration the energy band non-parabolicity effects. It was found that for most transitions studied the calculated interband energies exceed the experimental data by ~5-10 meV. This difference should be equal to exciton binding energy that was not included in our calculations. However, it is somewhat smaller than the exciton binding energies in undoped GaAs/AlAs QWs obtained from photoluminescence excitation studies [21]. Such differences could be related to many body effects [22].

**Exciton line broadening**

The DSPV spectra of GaAs/AlAs MQWs (Figs. 5 and 7) include a large number of well-resolved features associated with higher-energy QW transitions. Using this spectroscopic data, it is possible to extract information about the excitonic line broadening mechanisms and the interfacial properties, which define the quality of the structures studied. Figure 10 shows the dependencies of the broadening parameter Γ which represents the full width at half maximum (FWHM) of the exciton line on quantum number *n* determined from the lineshape analysis of DSPV spectra at 90 and 300 K for both weakly and strongly Be doped MQWs. Experimental data are presented for allowed heavy-hole related excitonic transitions. As can be seen from Fig. 10, at low temperature, the values of the broadening parameter of the ground state 11H excitonic transitions are almost the same for 1807 and 1392 samples and equal to 3±0.1 meV. At 300 K, the 11H exciton feature broadens to 8.7 meV in 1807 MQW and 12.5 meV in MQW structure 1392. Besides that, Fig. 10 shows that at both low and room temperature the exciton linewidth for sample 1807 increases with quantum

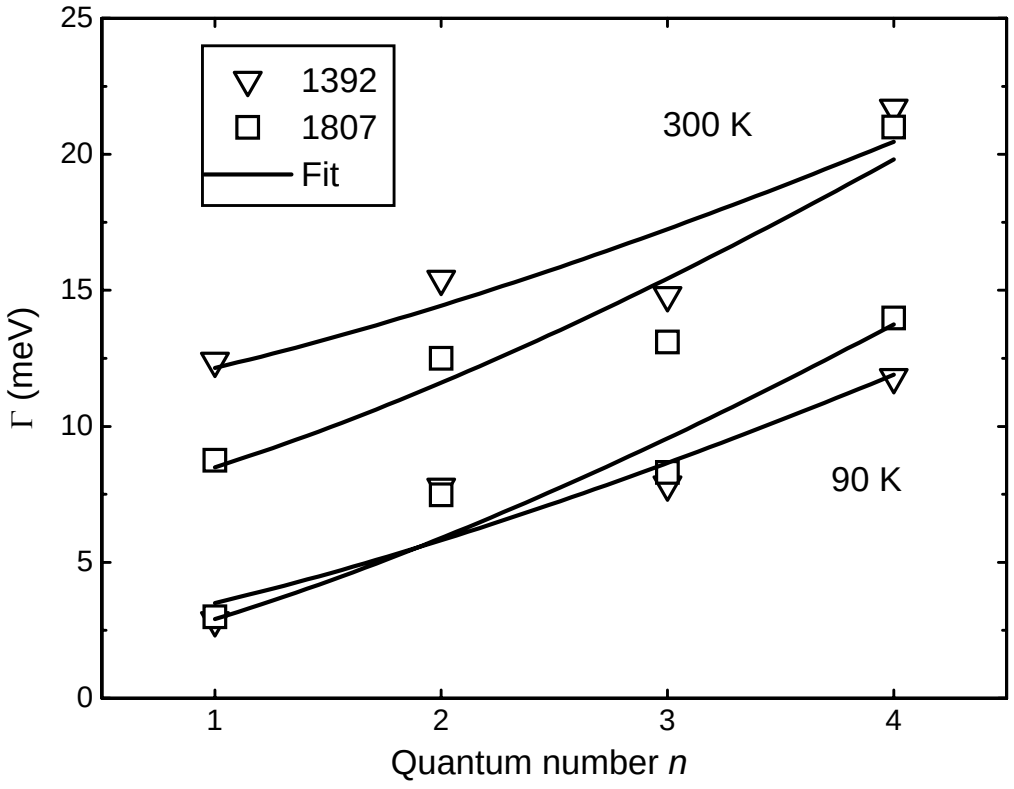


Fig. 10. Dependencies of the exciton linewidth Γ (FWHM) on quantum number *n*. Symbols – experiment, lines – fit to Eq. (3).

number *n* more rapidly when compared to sample 1392.

For Si doped GaAs/AlAs MQWs the Γ(*n*) dependencies are shown in Fig. 11. It should be noted that an increase of the excitonic linewidth with quantum number *n* is observed only for the lowest doping density sample L29. For more heavily doped samples L30 and L45 such an increase of the broadening parameter Γ is barely visible.

By interpreting experimental linewidth results, the interplay of several broadening mechanisms can be considered: temperature-independent inhomogeneous broadening of the exciton energy levels ($\Gamma_{inh}$) caused by structural imperfections in the QWs, such as interface roughness or composition fluctuations in the alloy and temperature-dependent homogeneous broadening ($\Gamma_{hom}$) due to exciton-phonon interaction, exciton scattering by ionized impurities and free carriers. The inhomogeneous broadening component $\Gamma_{inh}$ due to well width fluctuations is usually estimated from the experimental dependencies Γ(*n*) because this component predominantly causes the increase of Γ with *n* [23]. This effect can be understood considering $\Gamma_{inh}$ as the change

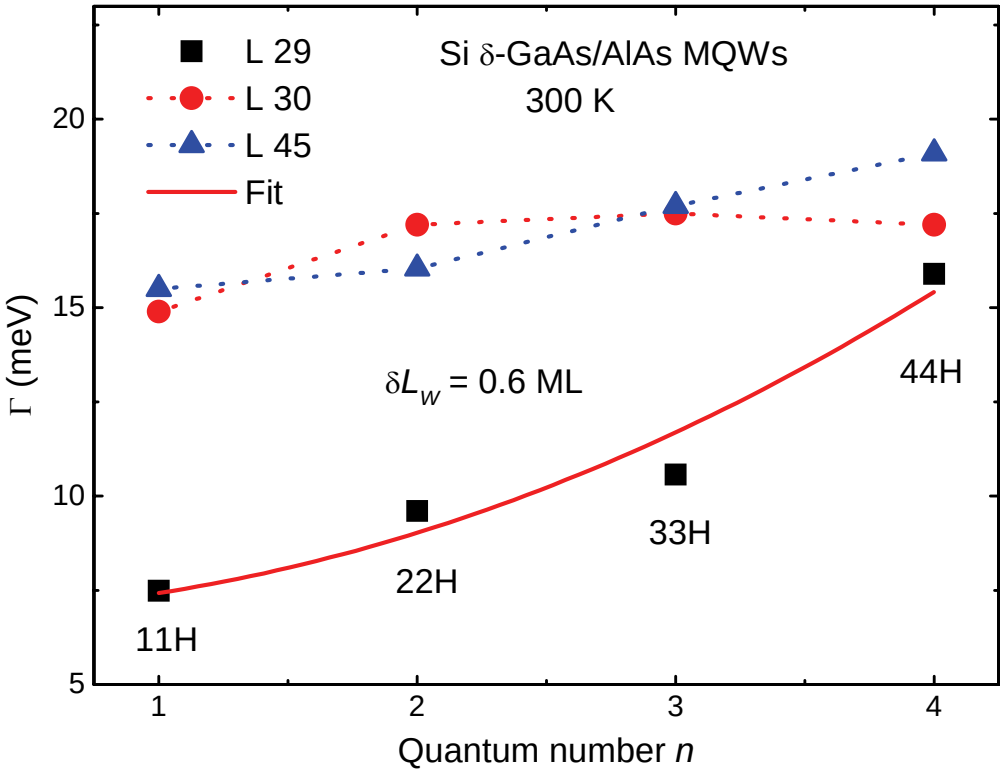


Fig. 11. The evolution of the broadening parameters Γ(FWHM) of heavy-hole related optical transitions as a function of the quantum number *n* in differently Si doped GaAs/AlAs MQWs.

of the exciton energy $E_n$ with any variation of the well width $L_w$ [11]

$$\Gamma_{inh}(n) = 2.36\ (dE_n/dL_w)\ \delta L_w, \qquad (3)$$

where $\delta L_w$ is the standard deviation of the well width fluctuations obeying a Gaussian distribution and $n$ is the quantum number of the QW subbands. In the case of QW systems with infinite potential barriers the derivative $dE_n/dL_w$ is proportional to the square of quantum index $n$ and $L_w^{-3}$ and can be expressed as

$$dE_n/dL_w = (\hbar^2\pi^2/\mu L_w^3)\ n^2 \qquad (4)$$

where $\hbar$ is Planck's constant and $\mu$ marks the reduced mass of the electron and hole. For finite barrier QW systems the relation (4) does not hold exactly because the energies of the excited states are usually lowered due to penetration of the wave functions into the barriers and also by band non-parabolicity effects. However, it clearly demonstrates that higher order optical transitions are more sensitive to the interface roughness in heterostructures than the ground state ones. This peculiarity of $\Gamma(n)$ we used to estimate the interface roughness in QWs for 1807, 1392 and L29 samples. Note that it is difficult to define an interface roughness in the Si doped samples L30 and L45 because there is no clear $\Gamma(n)$ dependence (Fig. 11).

The values of $\delta L_w$ characterizing the interface roughness in MQWs were evaluated from the broadening of the higher order quantum confined transitions by examining experimental $\Gamma(n)$ dependencies (Fig. 10, 11) with the relation

$$\Gamma(n) = a + \Gamma_{inh}(n), \qquad (5)$$

where the parameter $a$ contains all homogeneous broadening ($\Gamma_{hom}$) contributions. In this analysis, $\delta L_w$ and $a$ were treated as adjustable parameters while the derivatives $dE_n/dL_w$ were calculated numerically using a finite square-well potential approximation and taking into account the non-parabolicity of the energy bands.

From best fits of the experimental data to Eq. 5 (Fig. 10, 11, solid lines), the well width fluctuations $\delta L_w$ were found to be equal to ~0.6, ~ 0.8 and ~1.0 monolayer (1 ML = 2.83 Å) in samples L29, 1392 and 1807, respectively. Note, that the higher $\delta L_w$ values correspond to the MQW structure 1807 which has a larger number of periods (N=100) compared with the structure 1392 consisting of 40 periods. This observation implies that variations in width from well to well in addition to fluctuations within the same well occur in the structures under study. The values obtained for $\delta L_w$ are typical for GaAs/AlAs QW systems and show good interface quality for the samples studied.

It should be noted that the evaluated inhomogeneous broadening $\Gamma_{inh} \leq 1$ meV for 11H excitons is a non-dominant spectral line broadening mechanism both at low and room temperatures. Therefore, the other contributions should be important. The thermal exciton line broadening may be evaluated taking into account that exciton-acoustic phonon interaction coefficient: for GaAs/AlGaAs QWs this is estimated to be in the range $\gamma_{ac} \approx$ 1.6-10 μeV/K [24] and the exciton-LO phonon interaction coefficient $\gamma_{LO} \approx$ 8-15 meV [25, 26]. According to these coefficients, the spectral linewidth due to exciton scattering by acoustic phonons, $\Gamma_{ac}$, is expected to be ~0.14-0.9 meV at 90 K and ~0.5-3 meV at 300 K while broadening due to scattering by optical phonons, $\Gamma_{LO}$, should be important only at room temperature and could reach ~2.6-5 meV. However, taking even highest expected values of $\Gamma_{ac}$ and $\Gamma_{LO}$, the total linewidth for 11H excitons arising from thermal ($\Gamma_{th} = \Gamma_{ac} + \Gamma_{LO}$) and inhomogeneous ($\Gamma_{inh}$) broadening falls below the experimental values of Γ for sample 1392 at 295 K, but is comparable to Γ for sample 1807 at the same temperature. The evaluated total linewidth at 90 K is also found to be somewhat smaller (by about 1 meV) than the experimental one (Fig. 10). These observations imply that in weakly doped structures exciton-LO phonon scattering is the dominant mechanism of spectral line broadening at room temperature. The enhanced broadening in highly doped MQWs at 300 K allows us to suggest that it may be due to the contribution of exciton scattering by ionized acceptors and free holes. Surprisingly, at 90 K comparable Γ(*n*=1) values were found for samples 1807 and 1392 (Fig. 10), despite their very different acceptor densities. To explain this effect, it is proposed that the Coulomb potential of the charged acceptors, located within the plane of δ-layer, is screened at low temperature by free holes [27]. Therefore, the exciton scattering by ionized impurities may be suppressed.

From a comparison of the excitonic linewidth for Be and Si doped MQWs (Fig. 10, 11), it follows that Si doping more effectively broadens the lowest energy quantum states. The total linewidth of 11H and 22H transitions at 300 K in Si doped L30 and L45 samples is 2-3 meV larger than that in the more Be doped sample 1392. Furthermore, in the quantum number range from 1 up to 4, the value of Γ is roughly the same for samples L30 and L45. This suggests that the effect of disorder caused by the impurity sheet in the QW, which counteracts with the well width fluctuations induced effect, is more pronounced in Si doped MQWs.

## Optical properties of δ-doped GaAs/AlAs quantum wells:

## Study by photoluminescence and fractional dimensions approach

The properties of QWs are strongly influenced by the presence of doping impurities. The study of impurity-induced effects has both a fundamental interest and is of major importance in novel device applications such as high electron mobility transistors and QW infrared photodetectors/emitters.

Variations in the properties can be caused by changing the concentration of the dopant from uniform distributions across the QW width to concentrated sheet layers resulting in a so-called δ-doped profile. The energetic spectrum of an impurity in the QW is dependent on QW width, barrier height, impurity position and impurity concentration. Therefore, by changing the design of the structure and the doping profile, it is possible to tune in a controlled way the energetic levels. As a general rule, the impurity spectrum lies in the range of several meVs. In other words, these energies are within the THz range where the development of compact infrared emitters and small-size detectors is still an important issue.

The majority of previous works have mainly been focused on barrier-doped (selectively or modulation-doped) structures; in contrast, properties of doped QWs, in particular for the case for acceptor doping, are less understood. In this study, we have applied the fractional dimensional space (FDS) technique to beryllium acceptor states in GaAs/AlAs MQWs. We have shown that we can describe the excitonic spectrum, interband and beryllium acceptor related transitions, by the FDS approach and deduce the influence of *p*-doping effects on the optical properties of QWs having different widths and doping levels.

The FDS approach [28] was firstly applied by He [29-31] to study optical properties of anisotropic materials. FDS was found to be a powerful tool to examine the lineshape of the interband optical transitions and to elucidate the physical mechanisms defining the anisotropy of the system.

Impurities can be considered as hydrogen-like atoms and thus the FDS approach can be extended to describe these systems. In that case the discrete bound-state energies and orbital radii for excitons and impurities can be given by [31]:

$$E_n = \frac{R_y}{\left[n + \frac{\alpha - 3}{2}\right]^2}, \tag{6}$$

$$a_n = a_0\left[n + \frac{\alpha - 3}{2}\right]^2, \tag{7}$$

where $n$ =1, 2,… is the principal quantum number, $R_y$ and $a_0$ denote the Rydberg energy and Bohr radius for exciton or hydrogen-like impurity in the 3$D$ case, and $\alpha$ labels the dimensionality parameter which changes from 2 to 3 for idealized QWs. For the 2$D$ case, when $\alpha$ = 2, the binding energy of the 1s exciton or impurity is a factor of four greater than for the 3$D$ case, i.e. $E_1 = 4R_y$. (see for more details, e.g, [32]).

To analyze the excitonic photoluminescence spectra we have used a dimensionless absorption coefficient (optical density), which was theoretically deduced in $\alpha D$ space in [33, 34]:

$$O(\hbar\omega) = O_0\left[\sum_{n=1}^{\infty}\frac{4R_{y_{ex}}\Gamma(n+\alpha-2)}{(n-1)!\left(n+\frac{\alpha-3}{2}\right)^{\alpha+1}}\delta(\hbar\omega - E_n) + \left|\Gamma(\frac{\alpha-1}{2}+i\gamma\right|^2 e^{\pi\gamma}\frac{\gamma^{2-\alpha}}{\pi}\Theta(\hbar\omega)\right], \tag{8}$$

$\Theta(\hbar\omega)$ represents the Heaviside step function, $\gamma = \sqrt{R_{y_{ex}}/\hbar\omega}$, $\hbar\omega$ is the photon energy, $\alpha$ designates dimensionality and

$$O_0 = \frac{2^{2\alpha-3}e^2\left|d_{cv}\right|^2 L_c^{\alpha-2}}{\pi^{(\alpha-3)/2}n_B c m_0^2\omega}\frac{\left[\Gamma\left(\frac{\alpha}{2}\right)\right]^2\Gamma\left(\frac{\alpha-1}{2}\right)}{a_{0ex}^{\alpha}R_{y_{ex}}\left[\Gamma(\alpha-1)\right]^3}, \tag{9}$$

where $\omega$ is angular frequency of the incident light, $n_B$ is the refractive index of the medium, $m_0$ denotes the free electron mass, $e$ is electronic charge, $c$ stands for the velocity of light, $L_c$ labels the effective length of the active medium, $\left|d_{cv}\right|^2$ is the conduction-to-valence squared matrix element of the electron dipole moment and $\Gamma(x)$ denotes Euler's Gamma function.

The measurable dimensionless absorption coefficient including the Lorentzian line shape with full-width at half-maximum $w$ can be calculated from:

$$K_{ex} = \int_0^{\infty} O(\hbar\omega - E)\frac{2w}{\pi\left(4E^2 + w^2\right)}dE\,. \qquad (10)$$

The luminescence intensity $I_{PL}(E)$ is related to the absorption coefficient $K(E)$ through the energy balance relation

$$I_{PL}(E) \propto K(E)\,f(E)\,, \qquad (11)$$

where $f(E)$ is a suitable thermal function. In the limit of non-degenerate carrier density, $f(E)$ can be approximated by a Boltzmann distribution function.

In order to describe the shape of the spectrum it is of particular importance to evaluate the dimensionality parameter $\alpha$ of the confined exciton in the QW. There are several ways to proceed with this problem. For example, in Ref. 32, a simple definition of $\alpha$ on the well width for excitons is proposed:

$$\alpha_{ex} = 3 - \exp\left(-\frac{L_W}{2a_{ex}}\right), \qquad (12)$$

where $L_W$ represents the well width and $a_{ex}$ is the effective exciton Bohr radius. This equation is valid for infinite QWs. For real QWs with finite potential barriers, it can only be used for large QWs comparable to the infinite barrier theoretical device. The microscopic approach for $\alpha$ is proposed in Ref. 35, where one takes into account the penetration of the carriers into the barriers and incorporates the continuous interpolation of the material parameters from their values in the well region to their values in the barrier regions. The second option is to directly calculate the approximate values of $\alpha$ by solving the Schrödinger equation in $\alpha D$ space, as was suggested in Ref. 36. However, this method is rather complicated when it comes to interpreting the experimental results, since it requires additional theoretical calculations for all the particular QWs. Therefore, a more convenient way to obtain a dimensionality parameter is to use experimental data or other theoretical methods to calculate values of the exciton binding energies as a function of the well width. The dimensionality can then be determined directly by using Eq. 6.

The absorption coefficients of the interband optical transitions were calculated using the complex dielectric function from Ref. 30:

$$K_{b-b} = \frac{2^{3-\alpha}\pi^{2-\alpha/2}e^2\left|d_{cv}\right|^2 L_c^{\alpha-2}}{\Gamma\left(\frac{\alpha}{2}\right)n_B c m_0^2 \omega}\left(\frac{2\mu_{cv}}{\hbar^2}\right)^{\alpha/2}\sum_{\nu}\left(\hbar\omega - E_{QW}^{\nu\nu}\right)^{\frac{\alpha}{2}-1}\Theta\left(\hbar\omega - E_{QW}^{\nu\nu}\right), \qquad (13)$$

where $\mu_{cv} = m_c^* m_v^* / \left( m_c^* + m_v^* \right)$ is the reduced effective mass of the electron and hole. Here $E_{QW}^{\nu\nu}$ is the energy gap between the ν'th subband of the conduction, and ν'th subband of the valence band.

The calculations for $L_W$ = 15 nm ($N_{\mathrm{Be}}$ = 2.5×10$^{12}$ cm$^{-2}$) of each transition observed in the PL spectrum together with the experimental data at liquid nitrogen temperature is presented in Fig. 12. The excitonic PL spectra and interband transitions were calculated by the FDS approach including Lorentzian convolution, whereas the lineshape of bound excitons [Be, X] was approximated by a Gaussian. The dimensionality was extracted using Eq. 6.

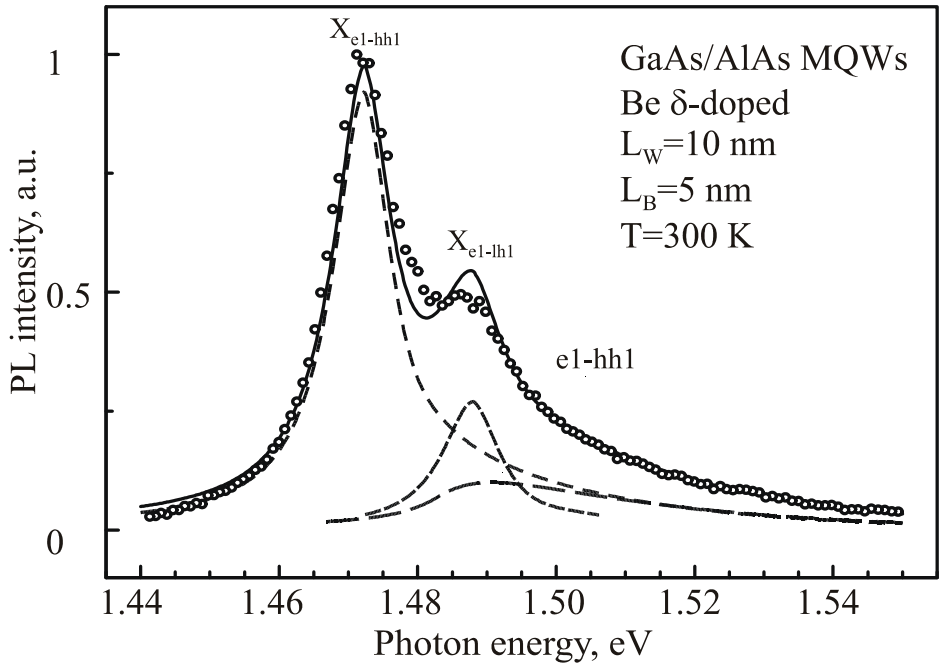


Fig. 12. The PL spectra of the δ-doped GaAs/AlAs MQWs with $L_W$ = 15 nm ($N_{\mathrm{Be}}$ = 2.5×10$^{12}$ cm$^{-2}$) at liquid nitrogen temperature. X$_{e1\text{-}hh1}$ and X$_{e1\text{-}lh1}$ indicate heavy-hole and light-hole excitonic transitions, [Be, X] labels exciton bound-to-Be acceptor, *e*-Be designates electron-neutral Be acceptor transitions, and *e*1-*hh*1 indicate electron-hole transitions. Dashed lines depict theoretical calculations; solid line represents the sum of all recombination mechanisms. The dimensionality, full-width at half-maximum of the Lorentzian or Gaussian convolution (given in parentheses) and relative weightings in the integrated PL spectra for various transitions are the following: *e*-Be (α = 2.87, $w_G$ = 6.4 meV) – 0.23; [Be,X] ($w_G$ = 4.7 meV) – 0.15; X$_{e1\text{-}hh1}$ (α = 2.3, $w_L$ = 3.5 meV) – 0.5; X$_{e1\text{-}lh1}$ (α = 2.2, $w_L$ = 3.5 meV) – 0.1; *e*1-*hh*1 (α = 2.3, $w_L$ = 3.5 meV) – 0.02.

In the modelling of the lineshape, we have assumed that the broadening of the excitonic PL linewidth consists of two components: a homogeneous and an inhomogeneous part:

$$\Gamma = \Gamma_0 + aT + b/[\exp(\hbar\omega_{LO}/kT) - 1], \qquad (14)$$

where $\Gamma_0$ is the temperature $T$ independent inhomogeneous width, while the second and third terms arise from the increase of the exciton scattering by acoustic and optical phonons with temperature, respectively. The coefficients $a$ and $b$ represent corresponding scattering strengths. As a general rule, the $\Gamma$ value is obtained from the measured PL spectra using Gaussian or Lorentzian convolution procedures.

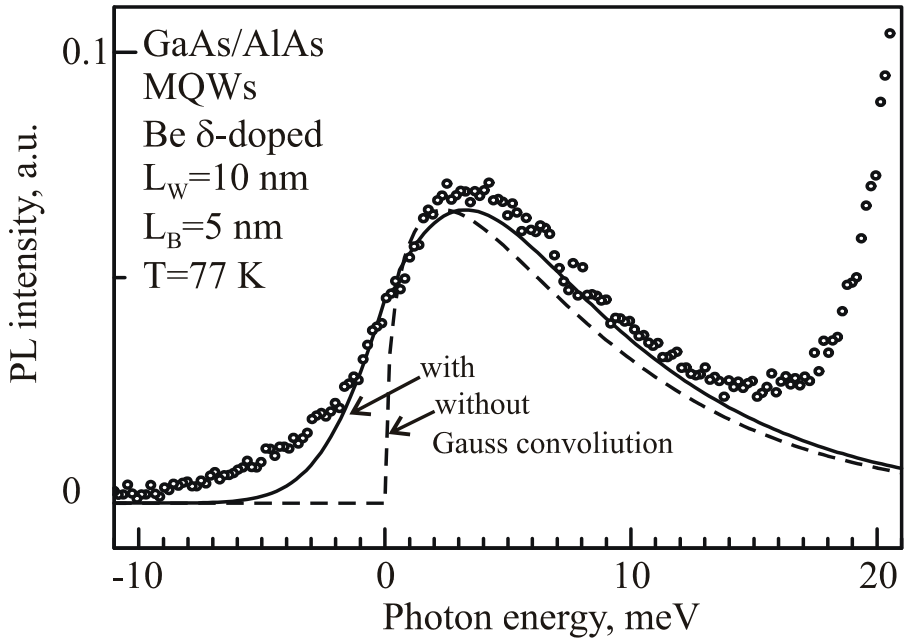


Fig. 13. The spectral shape of free electron-acceptor transition in $L_W$ = 10 nm width MQWs ($N_{Be}$ = 5×10$^{10}$ cm$^{-2}$) at liquid nitrogen temperature. Points show experimental data, lines denote theory: the dotted line is without and the solid line is with Gaussian convolution; the full-width at half-maximum is $w_G$ = 6 meV. Dimensionality $\alpha$ = 2.8. The energetic scale is relatively and shifted by the forbidden quantum well energy minus the acceptor binding energy.

The modelling results and the experimental data for the QW of 15 and 10 nm width at 77 K are presented in Fig. 12 and Fig. 13, respectively. It is clear that the use of a Gaussian convolution parameter with full-width at half-maximum $w_G$ = 6.4 meV for $L_W$ = 15 nm and $w_G$ = 6 meV for $L_W$ = 10 nm, provides excellent agreement with the

experimental results. In contrast, without the Gaussian convolution one can only approximate the high energy wing of the spectrum, while the low energy part in the simulations remains “step-like” (see Fig. 13), and hence does not fit into the experimental data. Knowing that dopants cause band edge fluctuations − so-called random potential or disorder − this effect, together with the phonon interaction, affects PL spectra inducing broadening in free electron-to-acceptor PL lineshape. The dimensionality was estimated from experimental acceptor binding energy, using formula

$$E_A = \boldsymbol{R}_{y_I}\left(\frac{2}{\alpha - 1}\right)^2 . \qquad (15)$$

Note that the lineshape of the transition is asymmetric. We suppose that this PL spectral feature is defined mainly by the spectral shape of the absorption coefficient and its product with the carrier distribution function. The influence of the energetically higher lying $\Gamma_7$ light-hole acceptor state on the PL spectral shape should be negligible because its splitting from the heavy-hole state amounts from only 0.55 meV up to 0.65 meV if the QW width decreases from 15 nm to 10 nm [37].

Finally, we will briefly comment on the influence of electron-phonon interactions on the threshold energy of the free electron-acceptor transition. We believe that the threshold energy and the acceptor binding energy are two different parameters. We have observed that the maximum of free electron-acceptor spectra is blue-shifted by a few meV from the threshold energy. However, we have ignored the electron-phonon interaction in our calculations which exhibit a strong effect in polar material such as GaAs. These interactions are known to cause longitudinal optical phonon (LO) sidebands which have been observed for the free electron-acceptor transitions in GaAs [38] and GaAs/AlAs MQWs [39]. The LO phonon interaction causes a red shift of the threshold energy, whose value is a few meV and there were an observed discrepancy between the threshold energy and acceptor binding energy in our experiments. This is the reason why, in order to overcome this effect, the true free electron-acceptor transition energy should be interpreted close to the maximum of the PL spectra.

Our experimental results and theoretical calculations are in excellent agreement with previous studies of the 3*D* case. One can clearly see that the FDS approach can be successfully used to analyze free-electron - acceptor impurities located in all positions of the QWs. The only condition that implies the impurities should be located

in a sheet and that their concentration should be low enough to provide no interaction between them. In this case our model can successfully be used to analyze free holes-to-donors transitions in QWs.

## CONCLUSIONS

1. We have designed various structures of δ-doped GaAs/AlAs MQW for optical, terahertz and electrical measurements.
2. Using DSPV spectroscopy, we have studied interband optical transitions, electronic structure and structural quality of Be and Si δ-doped GaAs/AlAs MQW samples designed for THz sensing applications. The energies of excitonic transitions and line broadening parameters for a large number of QW related transitions were determined from the line-shape analysis of DSPV spectra. The spectroscopic data of transition energies were found to be in agreement with calculations within the envelope function approximation which took into account the non-parabolicity of energy bands.
3. Analysis of the dependence of the exciton linewidth broadening on the quantum subband number allowed an evaluation of the line broadening mechanisms and interface roughness in the MQW structures.
4. In weakly Be-doped structures the exciton-LO phonon scattering is found to be the dominant mechanism of spectral line broadening at room temperature. The enhanced broadening in highly doped MQWs at 300 K may be due to contribution of exciton scattering by ionized acceptors and free holes. In Si-doped MQWs the doping broadens more effectively the lowest energy quantum states than doping with Be.
5. The average well width fluctuations were found to be ~0.6 – 1 ML and show good structural quality of studied samples.
6. Theory based on fractional dimensions to analyse impurity-related transitions was developed and applied for Be δ-doped GaAs/AlAs MQW samples; good agreement between experiment and theory is obtained.

**References**

[1] Y. M. Meziani, J. Lusakowski, N. Dyakonova, W. Knap, D. Seliuta, E. Širmulis, J. Devenson, G. Valušis, F. Boeuf, and T. Skotnicki, Program 6th

Topical Workshop on Heterostructure Microelectronics (TWHM−2005); Awaji Island, Hyogo, Japan, 22−25 August 2005; Comm. TuC-6, p. 54

[2] D. Seliuta, E. Širmulis, V. Tamošiūnas, S. Balakauskas, S. Ašmontas, A. Sužiedėlis, J. Gradauskas, G. Valušis, A. Lisauskas, H. G. Roskos, and K. Köhler, Electron. Lett. **40,** 631 (2004).

[3] H. Luo, H. C. Liu, C. Y. Song, and Z. R. Wasilewski, Appl. Phys. Lett. **86**, 231103 (2005).

[4] F.H. Pollak and H. Shen, Mater. Sci. Eng., R. **10**, 275 (1993).

[5] Y.S. Huang and F.H. Pollak, phys. stat. sol. (a) **202**, 1193 (2005).

[6] B. Čechavičius, J. Kavaliauskas, G. Krivaitė, D. Seliuta, G. Valušis, M.P. Halsall, M.J. Steer, and P. Harison, J. Appl. Phys. **98**, 023508 (2005).

[7] J. Misiewicz, P. Sitarek, G. Sęk, and R. Kudrawiec, Mater. Sci., **21**, 263 (2003).

[8] L. Kronik and Y. Shapira, Surf. Sci. Rep. **39**, 1 (1999).

[9] W. M. Sheng, M. P. Halsall, P. Harmer, P. Harrison, and M. J. Steer, Appl. Phys. Lett. **84**, 735 (2004).

[10] W.M. Zheng, M.P. Halsall, P. Harmer, P. Harrison, and M.J. Steer, J. Appl. Phys. **92**, 6039 (2002).

[11] K. K. Bajaj, Mater. Sci. Eng. *R* **34**, 59 (2001).

[12] S. Datta, S. Ghosh, and B. M. Arora, *Rev. Sci. Instrum.* **72**, 177 (2001).

[13] Yu. Kavalyauskas, G. Krivaite, A. Shileika, L. V. Sharonova, and Yu. V. Shmartsev, Semiconductors **27**, 598 (1993).

[14] P. Blood, J. Appl. Phys. **58**, 2288 (1985).

[15] R. Braunstein, P. Schreiber, and M. Welkowsky, Solid State Comm. **6**, 627 (1968).

[16] D.E. Aspnes, Surf. Sci. **37**, 418 (1973).

[17] V. Karpus, Two-dimensional electrons (Ciklonas, Vilnius, 2004), (in Lithuanian).

[18] B. Jonsson and S. T. Eng, IEEE J. Quantum Electron. **26**, 2025 (1990).

[19] Vurgaftman, J. R. Meyer, and Ram-Mohan, J. Appl. Phys. **89**, 5815 (2001).

[20] S. Adachi, J. Appl. Phys. **58**, R1 (1985).

[21] M. Gurioli, J. Martinez-Pastor, M. Colocci, A. Bosacchi, S. Franchi, and L. C. Andreani, Phys. Rev. B **47**, 15755 (1993).

[22] J. P. Loehr and J. Singh, Phys. Rev. B **42**, 7154 (1990).

[23] C. Bru-Chevallier, Y. Baltagi, G. Guillot, K. Hong, and D. Pavlidis, J. Appl. Phys. **84**(9), 5291 (1998).

[24] A.Thranhardt, C. Ell, S. Mosor, G. Rupper, G. Khitrova, H. M. Gibbs, and S. W. Koch, Phys. Rev. B **68**, 035316 (2003).

[25] D. Gammon, S. Rudin, T. L. Reinecke, D. S. Katzer, and C. S. Kyono, Phys. Rev. B **51**(23), 16785 (1995).

[26] A.Venu Gopal, R. Kumar, A. S. Vengurlekar, A. Bosacchi, S. Franchi, and L. N. Pfeiffer, J. Appl. Phys. **87**, 1858 (2000).

[27] R. N. Riemann, C. Metzner, and G. H. Döhler, Phys. Rev. B **65**, 115304 (2002).

[28] F. H. Stillinger, J. Math. Phys. **18**, 1224 (1977).

[29] X. F. He, Solid State Commun. **75**, 111 (1990).

[30] X. F. He, Phys. Rev. B **42**, 11751 (1990).

[31] X. F. He, Phys. Rev. B **43**, 2063 (1991).

[32] H. Mathieu, P. Lefebvre, and P. Christol, Phys. Rev. B **46**, 4092 (1992).

[33] P. Lefebvre, P. Christol, and H. Mathieu, Phys. Rev. B. **48**, 17308 (1993).

[34] P. Lefebvre, P. Christol, and H. Mathieu, Superlatt. Microstruct. **17**, 19 (1995).

[35] P. Christol, P. Lefebvre , and H. Mathieu, J. Appl. Phys. **74**, 5626 (1993).

[36] Matos-Abiague, L. E. Oliveira, and M. de Dios-Leyva, Phys. Rev. B **58**, 4072 (1998).

[37] P. O. Holtz, Q. X. Zhao, A. C. Ferreira, B. Monemar, M. Sundaram, J. L. Merz, and A. C. Gossard, Phys. Rev. B **48**, 8872 (1993).

[38] Q. Huang and R. G. Ulbrich, J. Lumin. **99**, 19 (2002).

[39] J. Kundrotas, A. Čerškus, S. Ašmontas, G. Valušis, B. Sherliker, M.-P. Halsall, P. Harrison, and M.-J. Steer, Acta Phys. Pol. A **107**, 245 (2005).

# Compact solid state terahertz detectors: Optical properties of active quantum structures and THz detection

Third interim report
Contract: FA8655-06-1-3007

# Introduction

The Terahertz (THz) ($1-10\times10^{12}$ Hz or equivalently 300−30 $\mu$m wavelengths) region of the electromagnetic spectrum lies between microwaves (exploited in mobile phones, satellite communications, television) and the infrared (used in heat sensing, short-range data communications) and is still largely unexplored and unexploited. This is despite large potential applications in such areas as bio-medical imaging (diagnosis of melanomas, drug levels in blood, DNA profiling, detection of bacterium and viruses), detection of chemical signatures (airport security, food hygiene, textiles) and satellite communications, to name but a few. The main obstacle in the development is just a characteristic of this frequency range – here the well-known principles of both photonics and electronics are no longer applicable. That is why a development of compact THz devices requires the confluence of various technologies and the establishment of novel principles.
Quite recently, the *THz Atelier* group from Vilnius, in co-operation with groups in Frankfurt/M (Germany) and Montpellier (France) has explored two principles devoted to broad band terahertz detection using semiconductor nanostructures containing two-dimensional electron gases (2DEG). The first way is to excite plasma waves in the 2DEG layer embedded in a field-effect transistor (FET) with submicron length gate. For instance, in CMOS transistors with a gate length of 30 nm the detection is at 2.52 THz [1]. The other approach is via non-uniform carrier heating in a 2DEG layer in GaAs/AlGaAs modulation doped structures in specifically engineered devices. These so-called bow-tie diodes (due to similarity of their shape to a bow-tie antenna) reveal a bandwidth of operation within the 10 GHz−2.52 THz range[2]. The inherent feature of the diodes is a *plateau* in voltage sensitivity across the 10 GHz−0.8 THz range with a value around 0.3 W/V. For direct applications, however, one needs to investigate a selective detection scheme which is free from selection rules limitation inherent for THz QWIPs (quantum well infrared photodetectors) devices [3].

This problem is the main inspiration of this work. The object of the investigation is *p* (Be)- and *n* (Si)- δ-doped GaAs/AlAs quantum wells with different well width and various doping levels. The study presents comprehensive research, both theoretical and experimental, by optical (modulation spectroscopy and photoluminescence), electrical and terahertz photocurrent techniques within 4−300 K temperatures.


1 Y. M. Meziani, J. Lusakowski, N. Dyakonova, W. Knap, D. Seliuta, E. Širmulis, J. Devenson, G. Valušis, F. Boeuf, and T. Skotnicki, Program 6th Topical Workshop on Heterostructure Microelectronics (TWHM−2005); Awaji Island, Hyogo, Japan, 22−25 August 2005; Comm. TuC-6, p. 54

2 D. Seliuta, E. Širmulis, V. Tamošiūnas, S. Balakauskas, S. Ašmontas, A. Sužiedėlis, J. Gradauskas, G. Valušis, A. Lisauskas, H. G. Roskos, and K. Köhler, Electron. Lett. **40,** 631 (2004).

3 H. Luo, H. C. Liu, C. Y. Song, and Z. R. Wasilewski, Appl. Phys. Lett. **86**, 231103 (2005).

# Design of Be and Si δ-doped GaAs/AlAs quantum wells

Delta-doped GaAs/AlAs multiple quantum wells (MQWs) were grown by molecular beam epitaxy (MBE) on semi-insulating (100) GaAs substrates with a 300 nm GaAs buffer. Each of the MQW structures investigated (samples designated as 1807, 1392, L 29, L 30 and L 45) contained 20 nm or 15 nm (samples 1303, L 79, L 151, L 152, L 153 and L 154) wide GaAs quantum wells (QWs) separated by 5 nm wide AlAs barriers. The QWs were δ-doped at the well centre with Be acceptor or Si donor atoms. The first 100-period GaAs/AlAs MQW structure (sample 1807) was weakly doped with acceptor density of $5\times10^{10}$ $cm^{-2}$. The second a 40-period MQW structure (sample 1392) was highly doped with Be acceptors of density $2.5\times10^{12}$ $cm^{-2}$. The 40-period MQW structures L29, L30 and L45 were relatively weakly doped with Si in the range from $4\times10^{9}$ to $1.4\times10^{11}$ $cm^{-2}$ and the structures were capped with a 100 nm GaAs layer. The doping level and the main characteristics of each sample are summarized in Table I.

**Table 1** Characteristics of the samples: the repeated period, the quantum well width ($L_w$), the δ-doping Be and Si concentrations ($N_A$) and ($N_D$), respectively, and the growth temperature of the epitaxial layer ($T$).

| Samples | Periods | $L_w$ (nm) | $N_A$ ($cm^{-2}$) | $T$ (ºC) |
|---|---|---|---|---|
| 1794 | 200 | 10 | $5\times10^{10}$ | 550 |
| 1303 | 50 | 15 | $2.5\times10^{12}$ | 540 |
| 1392 | 40 | 20 | $2.5\times10^{12}$ | 540 |
| 1807 | 100 | 20 | $5\times10^{10}$ | 550 |
| Samples | Periods | $L_w$ (nm) | $N_D$ ($cm^{-2}$) | $T$ (ºC) |
| L 29 | 40 | 20 | $4\times10^{9}$ | 670 |
| L 30 | 40 | 20 | $1.4\times10^{11}$ | 670 |
| L 45 | 40 | 20 | $5\times10^{16}$ ($cm^{-3}$) | 705 |
| L 79 | 50 | 15 | $5\times10^{12}$ | 700 |
| L 151 | 60 | 15 | $5\times10^{11}$ | 706 |
| L 152 | 60 | 15 | $5\times10^{10}$ | 710 |
| L 153 | 60 | 15 | $5\times10^{12}$ | 700 |
| L 154 | 60 | 15 | $9.99\times10^{12}$ | 700 |

*For sample L45, the Si doping was in the centre 2 nm of 20 nm GaAs quantum well.

The schematic band diagram of δ -doped GaAs/AlAs MQW structures was calculated from Poisson's equation. It was assumed that the surface Fermi level for *p*-type GaAs is pinned at 0.5 eV above the valence band. Consequently, this results in the formation of a surface depletion layer and a surface electric field. Another depletion layer is also formed at the interface between the MQW layer, and the substrate due to Fermi level pinning near midgap of the semi-insulating GaAs. The results of calculations for silicon doped QWs are given in Fig. 1.

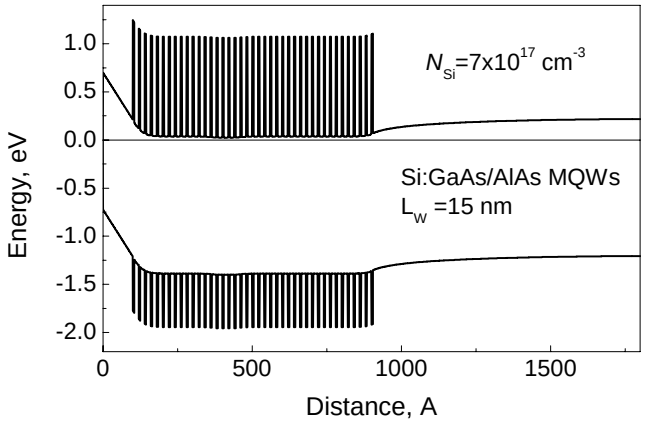


**Fig. 1.** Band diagram of Si δ-doped GaAs/AlAs MQW structure with width of 15 nm.

# Photoluminescence of δ-doped GaAs/AlAs quantum wells

The optical and electrical properties of quantum well structures are strongly influenced by the presence of doping. Despite detailed investigations of *n*-type doped quantum wells over a very broad doping range [1-4], questions still remain about the formation of impurity bands and the broadening of low energy tails in Si doped GaAs/$Al_xGa_{1-x}As$ quantum wells.

Impurities in quantum wells (QWs) can be distributed smoothly or be concentrated in a sheet – so-called δ-doping. The structure of the impurity spectrum also depends on the quantum well width, the barrier height, the impurity position, and the doping concentration [5-9]. In the case of highly δ-doped semiconductors or quantum wells, the interacting impurities form a new state leading to the creation of a two-dimensional carrier gas [10, 11].

For high impurity concentrations, photoluminescence (PL) spectra are limited by line broadening, and indeed recombination lines can merge obscuring the PL spectrum. Experimentally this problem cannot be resolved by reducing the lattice temperature as the line broadening is determined not only by phonons, but also by additional scattering mechanisms. These include the random distribution of impurities in the host lattice and interface roughness, which becomes predominant particularly for the case of narrow QWs.

It is generally accepted that high concentrations of impurities in semiconductors and QWs create tails in the distribution of allowed energy states, extending into the normally forbidden gap. As silicon is an amphoteric impurity in GaAs and GaAs/$Al_xGa_{1-x}As$ QWs, and can thus act as a shallow donor or a relatively shallow acceptor. The nature of the doping is dependent on the growth technique and conditions but, as a rule, typical molecular-beam epitaxial (MBE) growth conditions for Si-doped GaAs result in compensated *n*-type material. There is, however, still doubt on the origins of the compensation [12].

Here, we present results of an investigation the PL properties of highly Si δ-doped GaAs/AlAs multiple QWs at liquid nitrogen and room temperatures. We discuss possible mechanisms for carrier recombination in the QW structures placing particular emphasis on the origin of the low energy tail in the PL spectra, and its features.

## EXPERIMENTAL RESULTS

The PL spectra of the Si δ-doped MQWs are shown for different impurity concentrations in Figs. 2 and 3, for samples with well widths $L_W$, of 20 nm and 15 nm respectively. Data are shown (a) at room and (b) at liquid nitrogen temperatures. A series of clearly resolved PL peaks can be seen.

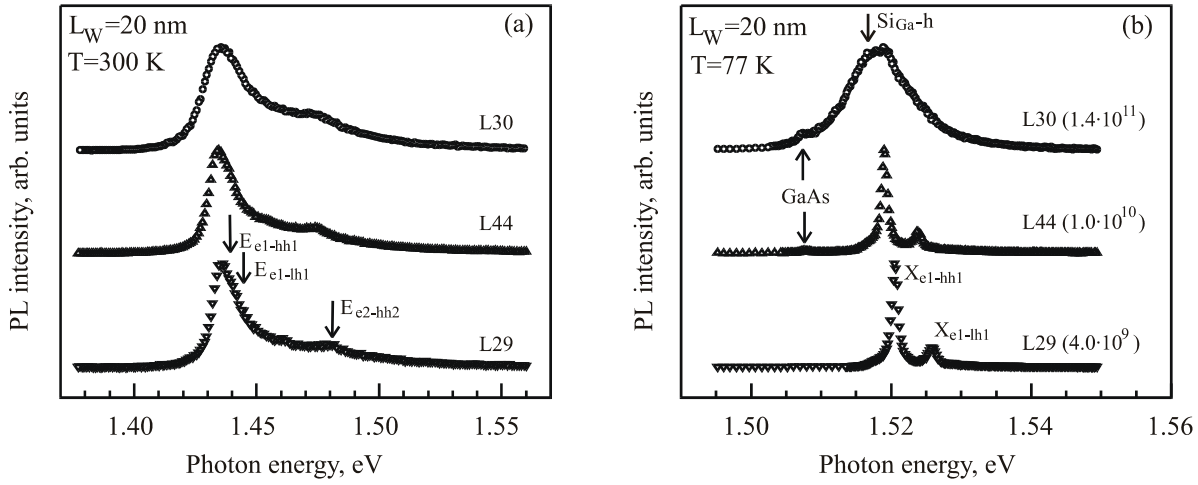


**Fig. 2.** PL spectra of the Si δ-doped GaAs/AlAs MQWs with well width $L_W$=20 nm at (a) room and (b) liquid nitrogen temperatures for various doping concentrations near the intrinsic transition region. Arrows in (a) indicate $E_{e1\text{-}hh1}$, $E_{e2\text{-}hh2}$, and $E_{e1\text{-}lh1}$, the calculated energy differences between the first heavy-hole and first electron, the second heavy-hole and second electron, and the first light-hole and first electron energy levels, respectively. $X_{e1\text{-}hh1}$ and $X_{e1\text{-}lh1}$ show heavy hole and light hole excitonic transitions, respectively. $Si_{Ga}$-*h* indicates the Si donor-free hole transitions and GaAs, the PL spectrum from the GaAs substrate. Brackets give Si concentration in units of $cm^{-2}$. The spectra have been shifted vertically for clarity.

In undoped and moderately Si doped samples, both heavy-hole and light-hole excitonic peaks (denoted as $X_{e1\text{-}hh1}$ and $X_{e1\text{-}lh1}$, respectively) are almost merged together at room temperature. At liquid nitrogen temperature, they became resolved as the most intense PL bands in the spectra. Arrows (Fig. 2 (a) and Fig. 3 (a)) indicate the calculated values of the sublevel energy differences of these PL transitions. The parameters used in the calculations are: a conduction-band-energy-discontinuity of $Q$=0.6; for GaAs an electron effective mass $m_e^*(\Gamma)/m_0$=0.0665, valence band Luttinger parameters $\gamma_1$=6.82 and $\gamma_2$=2.1, a forbidden energy gap $E_g(\Gamma, 300\ \mathrm{K})$=1.4256, and for AlAs $m_e^*(\Gamma)/m_0$=0.124, $\gamma_1$=4.04, $\gamma_2$=0.78, $E_g(\Gamma, 300\ \mathrm{K})$=3.02 [13].

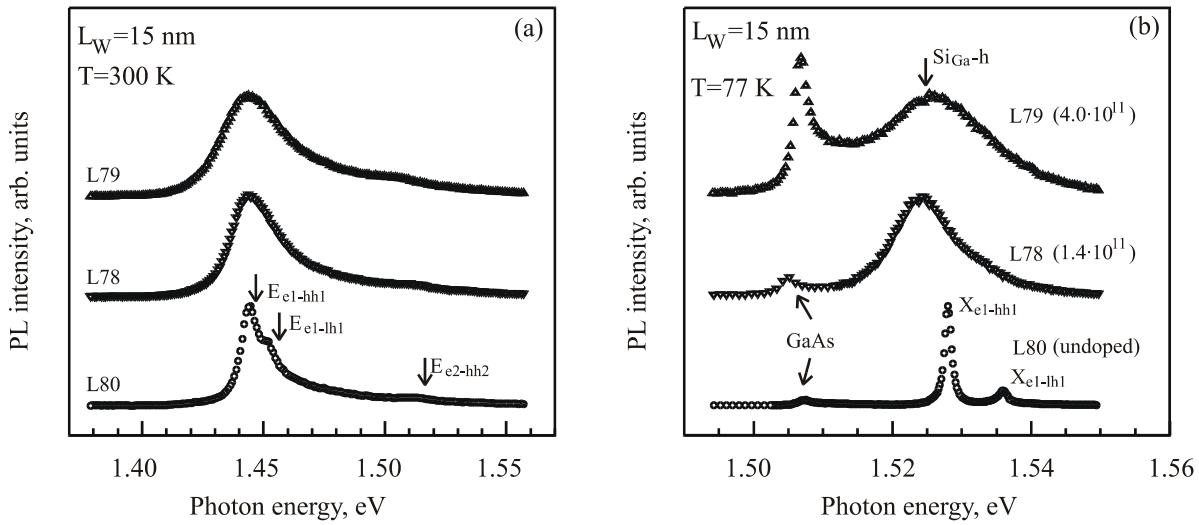


**Fig. 3.** PL spectra of the undoped and Si δ-doped GaAs/AlAs MQWs with well width $L_W$=15 nm at (a) room and (b) liquid nitrogen temperatures for various doping concentrations near the intrinsic transition region. The same symbols are used as in Fig. 2. The spectra have been shifted vertically for clarity.

From Figs. 2 and 3, it is clear that the spectra of highly doped samples are more complex, with the peak structure becoming more pronounced at 77 K. In addition to the peak arising from the substrate (marked as "GaAs" in Figs. 2 (a) and 3 (a)), an additional peak, indicated as $Si_{Ga}$-*h*, appears. This is assumed to relate to the Si donor--free hole transitions. It is worth noting that on the higher energy side of this transition, there are shoulders, the positions of which coincide with the heavy- and light-hole excitonic transitions of undoped or lightly doped samples. We deduce that the spectra for the highest doped sample arise from several constituents related to Si-donor related transitions and excitonic emissions.

The low energy tail of the PL spectra at liquid nitrogen temperatures for the Si δ-doped GaAs/AlAs MQWs with $L_W$=20 nm and 15 nm are shown in Figs. 4 (a) and 4 (b), respectively. In the same figures, for comparison, we have presented PL spectra of *p*-type Be δ-doped GaAs/AlAs MQWs, the spectral lines of which were clearly identified in [14]. The *p*-type spectra consist of a series of lines related to free electron-acceptor, or donor-acceptor and its LO-phonon replicas, transitions. It is seen that for undoped and weakly Si δ-doped samples the observed spectra are similar to Be δ-doped MQWs. This indicates that transitions related to residual donors, acceptors and their phonon replicas prevail in the spectra. However, for highly Si δ-doped samples, the low energy PL spectra changes drastically: Firstly, the PL emission is more intense in the low energy tail and the spectra loses its fine structure; secondly, we observe new bands at energies of 1.438 eV for $L_W$=20 nm and 1.442 eV for $L_W$=15 nm, which are marked as $Si_{Ga}$-$Ga_{As}$ transitions in Fig. 4.

The low energy tail PL spectra at 77 K are given in Fig. 5: (a) shows data taken in Si δ-doped GaAs/AlAs MQWs with $N_{Si}$=1.4·10$^{11}$ cm$^{-2}$ and $L_W$=20 nm various laser excitation intensity; while (b) part presents results on Si δ-doped GaAs/AlAs MQWs with $L_W$=15 nm ($N_{Si}$=1.4·10$^{11}$ and 4.0·10$^{11}$ cm$^{-2}$) for two laser excitation intensities. It can be noted that the energy positions of lines are independent of the laser excitation intensity; however, the relative PL intensity depends on the laser excitation intensity. For the bands marked as $Si_{Ga}$-$Ga_{As}$ we observe a tendency of saturation in the PL intensity at higher laser excitation levels.

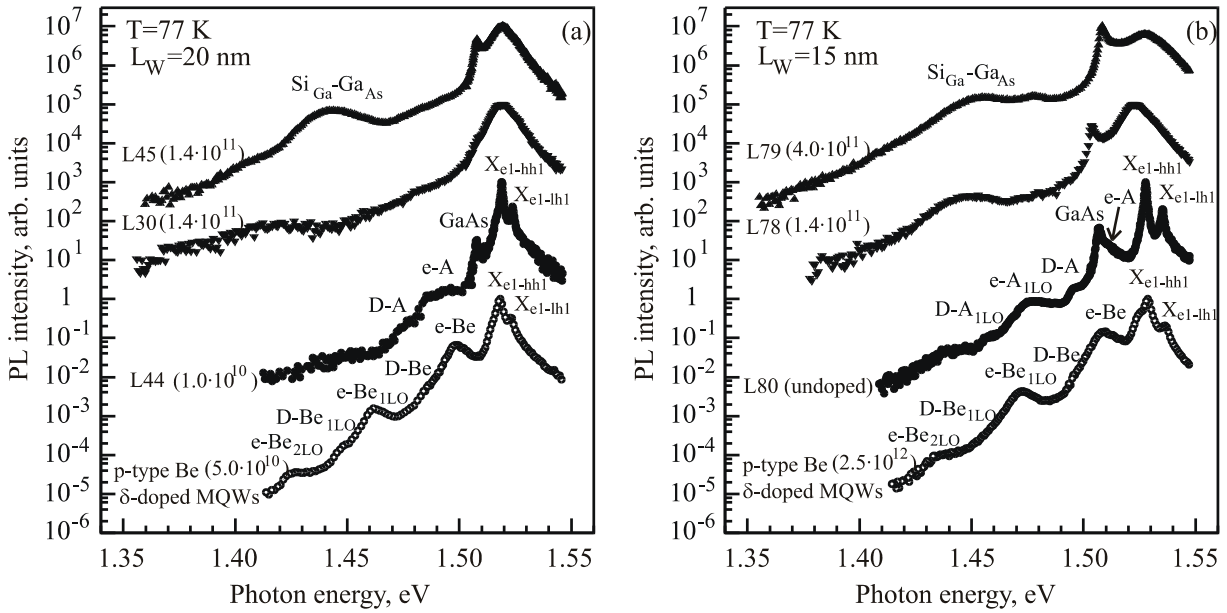


**Fig. 4.** The low energy tail PL spectra of undoped and Si δ-doped GaAs/AlAs MQWs with widths: (a) $L_W$=20 nm and (b) $L_W$=15 nm at liquid nitrogen temperature. *e-A* indicates the free electron-neutral acceptor transitions, and *D-A* the donor-acceptor transitions. For comparison the PL spectra of a Be δ-doped GaAs/AlGaAs MQW is shown for (a) $N_{Be}$=5.0·10$^{10}$ cm$^{-2}$ and (b) $N_{Be}$=2.5·10$^{12}$ cm$^{-2}$. Here, *e*-Be is the free electron-neutral Be acceptor transition, *e*-Be$_{1LO}$, *e*-Be$_{2LO}$ depict the first and the second phonon replica transitions, and *D*-Be and *D*-Be$_{1LO}$ indicate donor-Be acceptor and its phonon replica transitions. Si$_{Ga}$-Ga$_{As}$ marks the Si donor-antisite defect related transitions. Other symbols are as defined in Fig. 2. The spectra are shifted vertically for clarity.

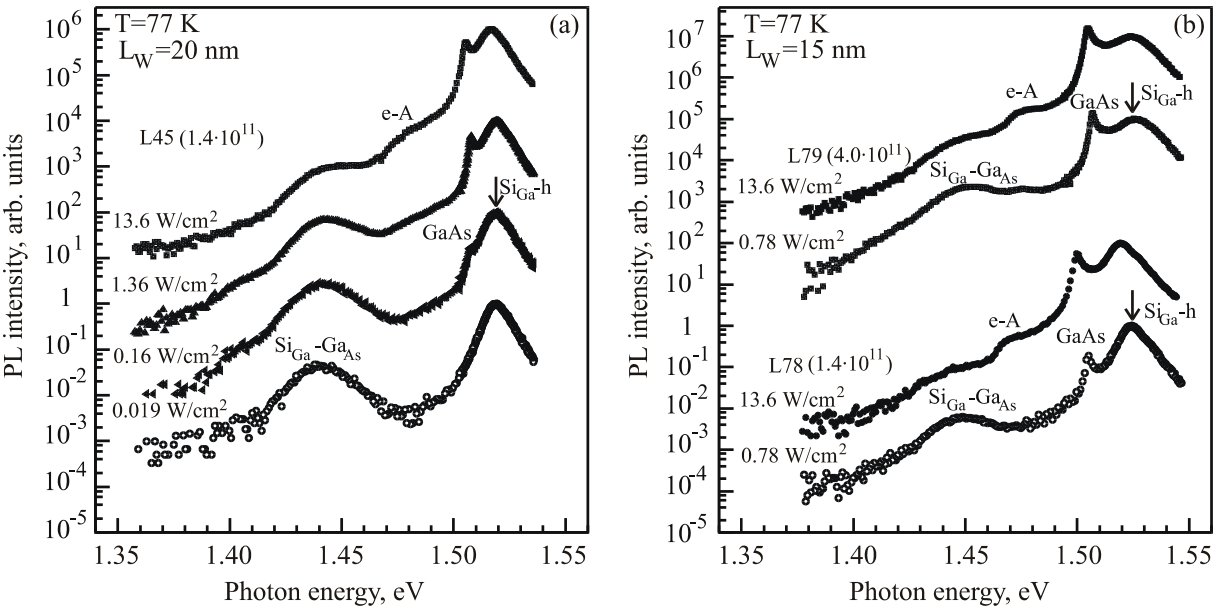


**Fig. 5.** The low energy tail PL spectra of the Si δ-doped GaAs/AlAs MQWs with (a) $L_W$=20 nm, and (b) $L_W$=15 nm at liquid nitrogen temperature for different laser excitation intensities. The notation is the same as in Figs 2 and 4. The spectra are shifted vertically for clarity.

## DISCUSSION

Impurities are fundamental to determining the electronic, optical and transport properties of QWs. Most of these properties depend on the doping level. A model assuming non-interacting impurities can explain the properties of weaker doped QWs. However, as the impurity concentration increases, one reaches a situation where single-impurity theory is no longer valid as the overlap of impurity wave functions becomes significant. At these concentrations is the start of the formation of the impurity band and the tail of the first conduction or valence subband edge, depending on the doping type. With further increases of

dopant concentration, an overlap of the broadened impurity band with the free carrier continuum occurs, making the impurity and conduction (valence) bands degenerate. This threshold corresponds to a transition from insulating to metallic behavior of the carriers – it is the so-called Mott transition [15]. In δ-doped QWs, where the impurity concentration is above the metallic limit the impurities begin to form a V-shaped potential well with a new two-dimensional subband structure.

In our analysis we assumed that the highly Si δ-doped GaAs/AlAs MQWs are non-degenerate, and their impurities are close to the Mott transition. As we observe shoulders in the spectra, which are consistent with excitonic transitions in the undoped or weakly doped samples, this indicates that the transformation of the sublevel system of the QW is minimal. It is known that in Si-doped MQWs excitons continue to dominate in the radiative recombination at doping levels right up to metallic limit [4]. The critical concentration for the insulator-metal transition and formation of subband structure, for δ-doping with donor impurity can be estimated from the relation [16]

$$N_I^{1/2} a_B \approx 0.31, \qquad (1)$$

where $N_I$ is the critical doping concentration [1/cm$^2$], and $a_B$ is the impurity Bohr radius [cm]. For QWs with $L_W$=20 nm and 15 nm, the donor activation energies are equal to about 9.4 and 10 meV, respectively [1, 6]. These values correspond to Bohr radii $a_D \approx 6.1$ nm and 5.8 nm, which leads to critical concentrations of $2.6 \cdot 10^{11}$ cm$^{-2}$ and $2.9 \cdot 10^{11}$ cm$^{-2}$. It was found experimentally that in *n*-type QWs the Mott transition occurs in the range $N_D = 2 \cdot 10^{11}$ - $4 \cdot 10^{11}$ cm$^{-2}$ [17]. Therefore, it might be that the change in the PL spectrum observed in our measurements at high doping levels can also be related to the Mott transition. However, this effect is definitely not enough to explain the rather broad low-energy tail in the PL spectra, which spreads over about 100 meV. Interpreting this effect within the traditional models of the formation of an impurity band and band tail is unsuccessful in the case Si doping, because these models give broadening energies of approximately a few Rydbergs [9]. It thus seems very likely that the effect is related to the amphoteric nature of Si as an impurity in GaAs: For high doping densities, a fraction of the Si dopants can occupy As sites and behave as acceptors. This self-compensation mechanism leads to fluctuations of conduction and valence bands – a so-called random potential – forming band-tail states. This model may help explain the luminescence properties of GaAs doped with Si impurities [18]. A similar effect might thus be expected in QWs doped with Si.

To complete the picture of the origin of the PL spectra, one needs to note that in highly doped samples we have also observed a new band, which is marked as $Si_{Ga}$-$Ga_{As}$ in Figs 4 and 5. To choose a possible model to interpret the formation of this band, we considered native and Si-related defects in GaAs. Six elementary native point defect species exist in GaAs: vacancies in the Ga sublattice ($V_{Ga}$), vacancies in the As sublattice ($V_{As}$), Ga self-interstitials, As self-interstitials, and antisite defects formed by a Ga atom on an As site ($Ga_{As}$) or an As atom on Ga site ($As_{Ga}$) [19]. Amongst the six intrinsic defects of GaAs, only $V_{Ga}$ and $Ga_{As}$ are acceptors [20]. For Si doped GaAs, it has been found that Si can behave as donor $Si_{Ga}$, an acceptor $Si_{As}$ and form Si pairs, clusters and complexes of Si atoms with native defects [12], which together can be responsible for self compensation mechanisms and creation of energy levels in the forbidden energy gap. From our experimental data, if we assume that we deal with donor $Si_{Ga}$-deep acceptor level transitions, we can find the acceptor binding energy (or acceptor band center energy) $E_A(Si_{Ga}\text{-}Ga_{As})$ from the relation

$$E_A(\mathrm{Si_{Ga}} - \mathrm{Ga_{As}}) = E(X_{e1-hh}) + E(X_{hh}) - E(\mathrm{Si}) - E(\mathrm{Si_{Ga}} - \mathrm{Ga_{As}}), \qquad (2)$$

where $E(X_{e1\text{-}hh1})$ and $E(Si_{Ga}\text{-}Ga_{As})$ are the energies of the $X_{e1\text{-}hh1}$ and $Si_{Ga}$-$Ga_{As}$ lines, and $E(X_{hh})$ and $E$(Si) are the binding energies of the heavy hole exciton and Si donor. For GaAs/AlAs QWs with $L_W$=20 nm and 15 nm, the heavy hole exciton binding energies are $E(X_{hh})$=8.2 and 9.6 meV respectively [21] and we deduce $E_A(Si_{Ga}\text{-}Ga_{As})$=78.8 and 79.6 meV. This energy is in agreement with $E_A(Si_{Ga}\text{-}Ga_{As})$=78 meV found for bulk Si doped GaAs [20, 22] and also observed in MBE grown Si-doped GaAs layers [23]. The inherent feature of this band is that it dominates the PL spectrum at low excitation power, but is quenched as the excitation power is increased [22]. We observed a similar effect in QW data shown in Figs 4 and 5. However, for one sample (L30) with a well width $L_W$ =20 nm and a doping level $N_{Si} = 1.4 \cdot 10^{11}$ cm$^{-2}$, we did not observe a $Si_{Ga}$-$Ga_{As}$ band in PL spectrum, see Fig. 4 (a). This could be related to the fact that this sample was grown at lower temperature since, generally, the formation of defects is very sensitive to the growth conditions [23].

Comparison of the PL spectra recorded in various QWs structures at 77 K are given in Fig. 6. The inherent feature of all the spectra is highly pronounced Be-impurity associated peak within 1.50-1.51 eV.

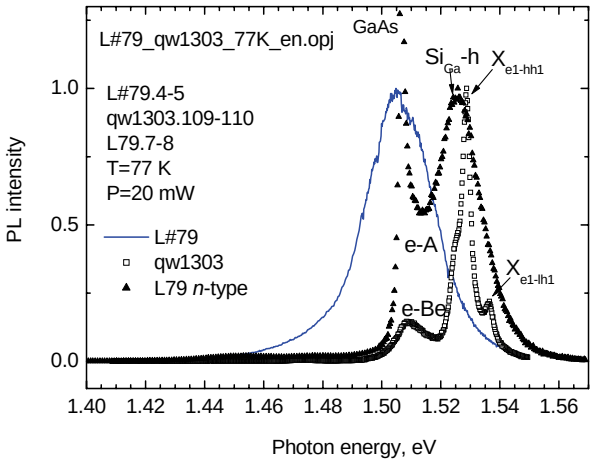


**Fig. 6a** Comparison of the PL spectra taken in various QWs.

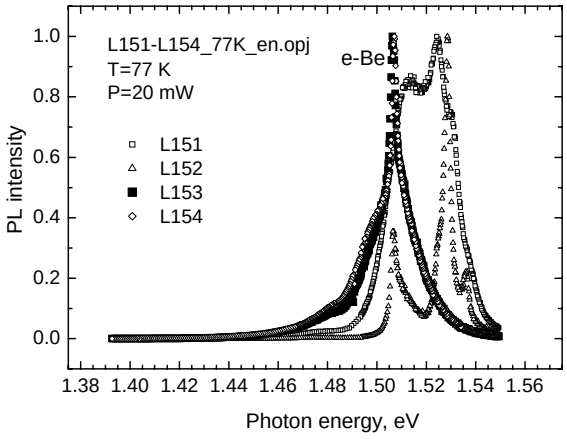


**Fig. 6b.** Comparison of the PL spectra taken in various *p*-type doped QWs

In summary, we have studied the influence of Si impurity concentration on the excitonic photoluminescence spectra of δ-doped GaAs/AlAs multiple quantum wells with widths $L_W$=20 and 15 nm, observing line broadening and the creation of donor $Si_{Ga}$- free hole and donor $Si_{Ga}$- acceptor $Si_{As}$ transitions. At high doping concentrations, we have also observed the formation of a low-energy PL tail, which is related to Si impurities in GaAs being amphoteric in nature. The low-energy PL tail contains an emission band which we attribute to transitions from a $Si_{Ga}$ donor to a deep *p*-type antisite defect $Ga_{As}$. The activation energy of this defect was found to be about 79 meV.

## REFERENCES


1. X. Liu, A. Petrou, B. D. McCombe, J. Ralston, and G. Wicks, Phys. Rev. B **38**, 8522 (1988).
2. R. Stepniewski, S. Huant, G. Martinez, and B. Etienne, Phys. Rev. B **40**, 9772 (1989).
3. D. C. Reynolds, K. R. Evans, C. E. Stutz, K. K. Bajaj, and P. W. Yu, Phys. Rev. B **44**, 8869 (1991).
4. C. I. Harris, B. Monemar, H. Kalt, and K. Köhler, Phys. Rev. B **48**, 4687(1993).
5. G. Bastard, Phys. Rev. B **24**, 4714 (1981).
6. C. Mailhiot, Yia-Chung Chang, T. C. McGill, Phys. Rev. B **26**, 4449 (1982).
7. R.L. Greene and K.K. Bajaj, Solid State Commun. **53**, 1103 (1985).
8. E. Reyes-Gómez, A. Matos-Abiague, C. A. Perdomo-Leiva, M. de Dios-Leyva, and L. E. Oliveira, Phys. Rev. B **61**, 13104 (2000).
9. J. Serre, A. Ghazali, and A. Gold, Phys. Rev. B **39**, 8499 (1989).
10. *Delta-doping of semiconductors*, Ed. E. F. Schubert (Cambridge University Press, 1996).
11. J. J. Harris, R. Murray, and C. T. Foxon, Semicond. Sci. Technol. **8**, 31 (1993).
12. S. Modesti, R. Duca, P. Finetti, G. Ceballos, M. Piccin, S. Rubini, and A. Franciosi, Phys. Rev. Lett. **92**, 086104 (2004).
13. J. Kundrotas, A. Čerškus, S. Ašmontas, G. Valušis, B. Sherliker, M. P. Halsall, M. J. Steer, E. Johannessen, and P. Harrison, Phys. Rev. B **72**, 235322 (2005).
14. J. Kundrotas, A. Čerškus, A. Johannessen, S. Ašmontas, G. Valušis, M.-P. Halsall, and P. Harrison, see Proc. of this Conference.
15. N. F. Mott, *Metal-insulator transitions*, (Taylor & Francis Ltd, London 1974).
16. J. Kortus and J. Monecke, Phys. Rev. B **49**, 17216 (1994).
17. M. Carras, V. Berger, X. Marcadet, and B. Vinter, Phys Rev. B, **70**, 233310 (2004).
18. D. Redfield, J.P. Wittke, and J. I. Pankove, Phys. Rev. B **2**, 1830 (1970).
19. N. H. Ky and F. K. Reinhart, J. Appl. Phys. **83**, 718 (1998).

20. L. Pavesi, N. H. Ky, D. Ganière, F. K. Reinhart, N. Baba-Ali, I. Harrison, B. Tuck, and M. Henini, J. Appl. Phys, **71**, 2225 (1992).
21. L.C. Andreani and A. Pasquarello, Phys. Rev. B, **42**, 8928 (1990).
22. I. Harrison, L. Pavesi, M. Henini, and D. Johnston, J. Appl. Phys. **75**, 3151 (1994).
23. M. Mihara, M. Mannoh, K. Shinozaki, S. Naritsuka, and M. Ishii, Jpn. J. Appl. Phys. **25**, L611 (1986).

## Photoreflectance spectroscopy of δ-doped GaAs/AlAs quantum wells

The results of the photoreflectance (PR) spectra within the range 1.35 – 1.70 eV for the *p*-type and *n*-type GaAs/AlAs MQW samples with various well widths and doping concentrations are given Fig. 7 and Fig. 8. The PR spectrum from an epitaxial *p*-GaAs layer is also shown for comparison in Fig. 7. As one can see, the PR signal exhibits oscillatory behavior above the band-gap energy of GaAs (1.424 eV). It was found that the oscillations are not related to the light interference fringes visible in reflectivity spectra (not shown) because its period could be reduced by the optical bias via the photovoltage effect. We attribute therefore the oscillatory features in PR spectra to the Franz-Keldysh oscillations (FKOs) originating due to internal electric fields in the samples [1, 2]. In addition to the FKOs, at higher energies, a number of *mn*H(L) features associated with the excitonic transitions in the MQW region of the samples are observed. The notation *mn*H(L) signifies here the transitions between the *m*-th electron and *n*-th heavy hole (H) or light hole (L) subbands. These features are more pronounced in the DSPV spectra of these samples and will be considered in detail later. Now, we will discuss the origin of the FKOs above the GaAs band gap energy.

According to the calculated band diagram, the FKO features in the structures studied may be induced by photo-modulation of the band bending near the surface in the GaAs cap layer, and/or near the interface in the GaAs buffer layer. Obviously, the effectiveness of the photo-modulation of the interfacial electric field is limited due to light absorption in the structure above the buffer layer. Therefore, the PR intensity

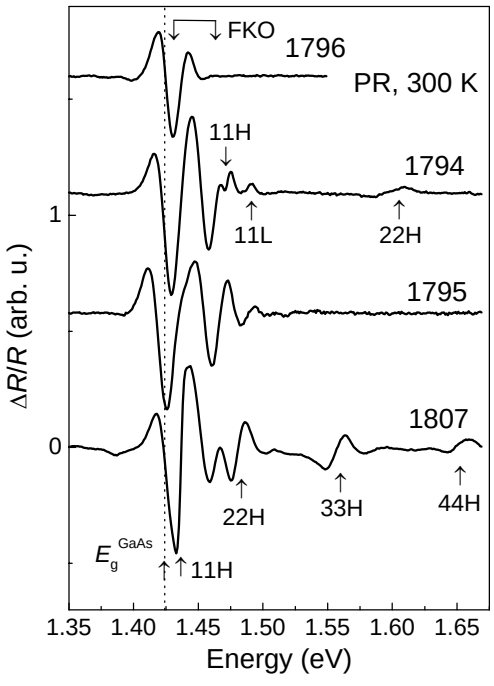


**Fig. 7.** Room temperature PR spectra of GaAs epilayer 1796 and δ-doped GaAs/AlAs MQW samples with different well widths. Arrows mark the energies of optical transitions. For the sake of clarity, the spectra of different samples are shifted vertically.

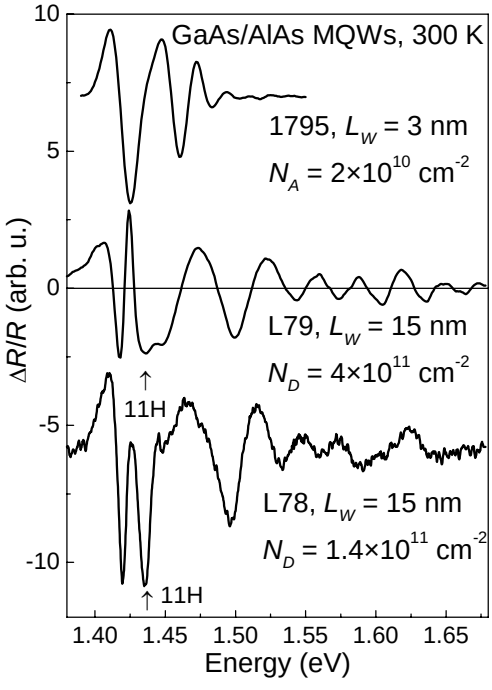


**Fig. 8.** Room temperature PR spectra of *p*-type (1795) and *n*-type (L78, L79) δ-doped GaAs/AlAs MQW samples having different well widths and doping density. Arrows mark the energies of optical transitions. The spectra obtained for the different samples are vertically shifted for clarity.

should be strongly dependent on the thickness of the mentioned structure as well as the wavelength (penetration depth) of the modulation light beam. Also, it is worth noting that the phase of FKOs

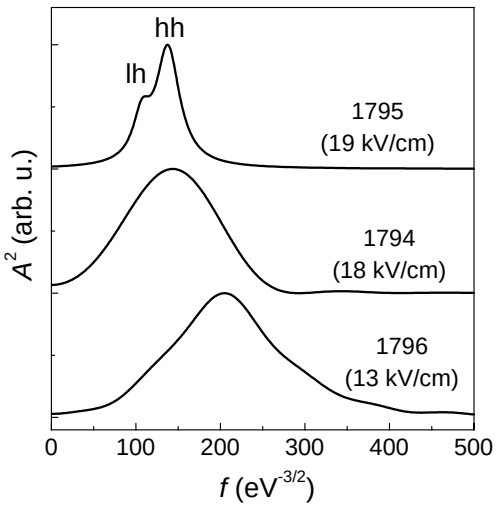


**Fig. 9.** Fourier transforms of the FKOs obtained from the PR spectra (Fig. 7) for samples Be-doped MQWs.

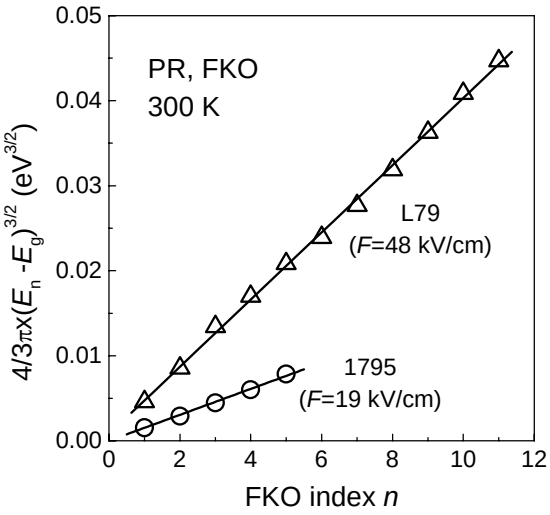


**Fig. 10.** Plots of the quantity $(4/3\pi)(E_n-E_g)^{3/2}$ versus index *n* of the FKOs for the Be- (1795) and Si- (L79) doped GaAs/AlAs MQWs.

originating from the buried interface shifts strongly with the change of the epilayer thickness due to an interference effect [3]. It is possible therefore to use these peculiarities to unveil the origin of the observed FKOs. More detailed consideration of the PR results, for instance, for samples 1807, 1794 and 1795 (Fig. 7) shows that the change in the thickness of the MQWs layer from 2.5 (sample 1807) to 3.2 μm (sample 1795) does not affect strongly the phase of the FKOs. Also, we have found that the phase and the period of the FKOs do not depend on the

wavelength (penetration depth) of the pump beams. Therefore, it could be inferred that the PR signals for these thick MQW samples arise mainly due to the photomodulation of the surface electric field. Calculations have shown that the structures studied should exhibit a nearly uniform electric field in the undoped GaAs cap layer and cause slowly decaying FKOs in the PR spectra. In contrast, due to the broadening effects and non-uniform electric field the FKOs are damped much faster in a doped epitaxial GaAs layer then in MQWs (Fig. 7).

By analyzing FKOs, it is possible to calculate the surface electric field. In such analysis, the oscillatory behavior of FKOs is described as [1]

$$\frac{\Delta R}{R} \sim \cos\left\{\frac{4}{3}\cdot\left[\frac{E-E_g}{\hbar\theta}\right]^{\frac{3}{2}}+\varphi\right\}, \qquad (1)$$

where $E$ is the photon energy, $E_g$ is the band-gap energy, $\hbar\theta=(e^2F^2\hbar^2/8\mu)^{1/3}$ is an electro-optic energy, $e$ is the electron charge and $\mu$ is the reduced mass of the electron and hole in the direction of the electric field $F$, $\hbar$ is Planck's constant and $\varphi$ is a phase factor which is influenced by inhomogenity of the internal electric field [2].

Following Eq. 1, the built-in electric field strength can be evaluated by fast Fourier transform (FFT) analysis of the FKOs in the energy region above the GaAs band gap [4]. Proceeding in this direction, the experimental PR spectrum has been renormalized substituting a new argument, $(E-E_g)^{3/2}$, and multiplying the spectrum by $E^2(E-E_g)$ in order to deal with periodic functions and compensate for the damping of the FKOs, respectively. Then, according to Eq. (1), the peak quasi-frequency $f$ of the band in the spectrum, evaluated from the Fourier transform of the FKO, is related to the electric field by

$$f=\frac{2}{3\pi}(\hbar\theta)^{3/2}=\frac{4\sqrt{\mu}}{3\pi}\cdot\frac{1}{e\hbar F}. \qquad (2)$$

The FFTs of the PR spectra of several of the GaAs/AlAs MQW structures are plotted in Fig. 9. For sample 1795, the two peaks of the FFT correspond to the heavy (hh) and light (lh) hole subband

contributions to the PR spectra. The ratio of frequencies $f_{hh}/f_{lh}$ = 1.29 is consistent with the ratio of $(\mu_{hh}/\mu_{lh})^{0.5}$. For other samples, only a single peak is seen in the transformed spectra arising from the more intense heavy hole-related band gap transition. These peaks are very broad due to the small number of FKOs in the PR spectra, and the signature of the light hole contribution is not resolved. The calculated surface electric fields using Eq. (2) are also presented in Fig. 9. The electric field values obtained in the cap layer of the MQW structures are about 20 kV/cm and are consistent with the calculated surface field value for an acceptor concentration of $2\times10^{17}$ $cm^{-3}$.

For comparison, we have also estimated the internal electric field *F* for Be- (1795) and Si- (L79) doped GaAs/AlAs MQW samples of different doping. This data was extracted using the relationship between the energy position $E_n$ of FKO extrema and the extremum index *n* and plotting the dependence of the quantity $(4/3\pi)(E_n-E_g)^{3/2}$ as a function of the index *n* (Fig. 10). From the slope of the straight lines the electric fields *F* were calculated according to Eq. 1. One can see from Fig. 10 that the surface electric field in *n*-type structures is much larger in comparison to *p*-type MQWs. This could be related to a larger surface potential value in the *n*-type samples.

## REFERENCES


1. D.E. Aspnes and A.A. Studna, *Phys. Rev. B.* **7**, pp. 4605-4625, 1973.
2. D.E. Aspnes, *Phys. Rev. B.* **10**, pp. 4228-4238, 1974.
3. H. Takeuchi, Y. Yamamoto, R. Hattori, T. Ishikawa, and M. Nakayama, *Jpn. J. Appl. Phys.* **42**, pp. 6772--6778, 2003.
4. D. P. Wang and C.T. Chen, *Appl. Phys. Lett.* **67**, pp. 2069-2071, 1995.


# Terahertz photocurrent spectroscopy of beryllium δ-doped GaAs/AlAs quantum wells

To test their operation within the THz range, we have measured the THz radiation-induced photocurrent in the in-plane geometry of the samples at helium temperatures. The results are depicted in Fig. 11. The origin of the signal we associate mainly with photothermal ionization of Be acceptors as the increase in photoresponse corresponds to the acceptor binding energy. Note that sample 1392 having two orders of magnitude higher doping, produced significantly higher signal because of an increase in THz absorption. The signal observed below 4 THz can be related to excited acceptor states $2P_{3/2}$ and $2P_{5/2}$ having transition energies several meV lower than the binding energy [1].

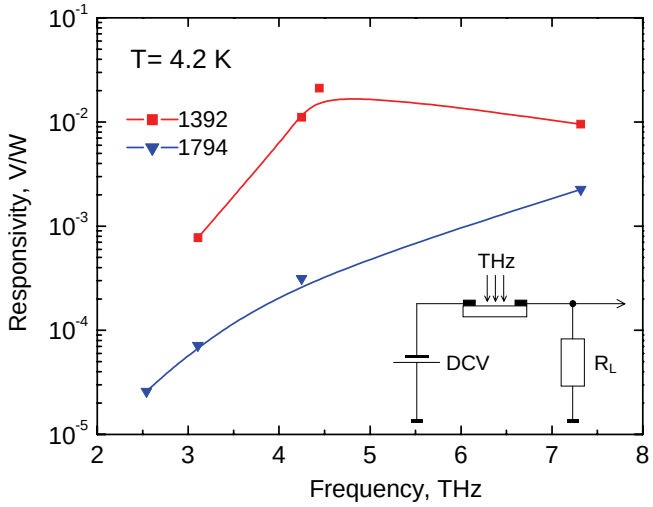


**Fig. 11** Photocurrent spectra of the δ-doped GaAs/AlAs MQW-based devices recorded within THz range at helium temperatures.

## REFERENCES


1. R.F. Kirkman, R. A. Stradling, and P.J. Lin-Chung, J.Phys. C, Solid State Phys. **11,** 419-433 (1978).